https://doi.org/10.5194/cp-2019-157
Preprint. Discussion started: 16 January 2020

Paleogeographic controls on the evolution of Late Cretaceous ocean circulation

Jean-Baptiste Ladant[1], Christopher J. Poulsen[1], Frédéric Fluteau[2], Clay R. Tabor[3], Kenneth G. MacLeod[4], Ellen E. Martin[5], Shannon J. Haynes[6], Masoud A. Rostami[7]

[1]*Department of Earth and Environmental Sciences, University of Michigan, Ann Arbor, MI, USA*
[2]*Institut de Physique du Globe de Paris, Université de Paris, CNRS, F-75005 Paris, France*
[3]*Department of Geosciences, University of Connecticut, Storrs, CT, USA.*
[4]*Department of Geological Sciences, University of Missouri, Columbia, MO, USA*
[5]*Department of Geosciences, Williamson Hall 362, University of Florida, Gainesville, FL, USA*
[6]*Department of Geosciences, Guyot Hall, Princeton University, Princeton, NJ, USA*
[7]*Ecology, Evolution and Conservation Biology Department, University of Nevada, Reno, NV, USA*

Abstract

Understanding of the role of ocean circulation on climate during the Late Cretaceous is contingent on the ability to reconstruct its modes and evolution. Geochemical proxies used to infer modes of past circulation provide conflicting interpretations for the reorganization of the ocean circulation through the Late Cretaceous. Here, we present climate model simulations of the Cenomanian (100.5 – 93.9 Ma) and Maastrichtian (72.1 – 66.1 Ma) stages of the Cretaceous with the CCSM4 earth system model. We focus on intermediate (500 – 1500 m) and deep (> 1500 m) ocean circulation, and show that while there is continuous deep-water production in the southwest Pacific, major circulation changes occur between the Cenomanian and Maastrichtian. Opening of the Atlantic and Southern Ocean, in particular, drives a transition from a mostly zonal circulation to enhanced meridional exchange. Using additional experiments to test the effect of deepening of major ocean

https://doi.org/10.5194/cp-2019-157
Preprint. Discussion started: 16 January 2020

gateways in the Maastrichtian, we demonstrate that the geometry of these gateways likely had a considerable impact on ocean circulation. We further compare simulated circulation results with compilations of ε_{Nd} records and show that simulated changes in Late Cretaceous ocean circulation are reasonably consistent with inferences from this proxy. In our simulations, consistency with the geologic history of major ocean gateways and absence of shift in areas of deep-water formation suggest that the Late Cretaceous trend in ε_{Nd} values in the Atlantic and southern Indian Oceans was caused by the subsidence of volcanic provinces and opening of the Atlantic and Southern Oceans rather than changes in deep-water formation areas and/or reversal of deep-water fluxes. However, the complexity in interpreting Late Cretaceous ε_{Nd} values underscores the need for new records as well as specific ε_{Nd} modeling to better discriminate between the various plausible theories of ocean circulation change during this period.

Introduction

Over the last several decades, a wealth of proxy data established that the Cretaceous period was characterized by a greenhouse climate, with warmer than modern temperatures and an absence of perennial polar ice sheets (e.g., Barron, 1983; Jenkyns et al., 2004; Friedrich et al., 2012; O'Brien et al., 2017). This characterization draws on paleontological and paleobotanical data, including the findings of fossils of ectothermic species (e.g., Tarduno et al., 1998) and woody vegetation (e.g., Bowman et al., 2014) at polar latitudes, as well as geochemical studies indicating warm sea surface and deep ocean temperatures at all latitudes (e.g., Wilson and Norris, 2001; Pucéat et al., 2003; Friedrich et al., 2012; MacLeod et al., 2013; O'Brien et al., 2017; Huber et al., 2018). Successive refinements of the data indicating Cretaceous warmth also reveal a greater variability within Cretaceous climates that includes carbon cycle perturbations referred to as ocean anoxic events (OAE, e.g., Schlanger and Jenkyns, 1976; Jenkyns, 2010) and intervals of cooler climatic conditions indicated by evidence for polar sea ice (Davies et al., 2009; Bowman et al., 2013) and possibly short-lived polar ice sheets (Price, 1999; Ladant and Donnadieu, 2016). Global temperature compilations confirm this long-term variability and provide evidence of long-term global warming through the Early Cretaceous to early Late Cretaceous (Cenomanian-Turonian) interval of maximum temperatures followed by cooling through the end of the Cretaceous (Cramer et al., 2011; O'Brien et al., 2017; Huber et al., 2018).

Early attempts at modeling past climates with atmosphere-only global climate models suggested that Cretaceous warmth was the result of paleogeographic changes and higher atmospheric CO_2 concentrations (Barron and Washington, 1982, 1984, 1985). The role of paleogeographic changes on global temperature evolution across the Cretaceous has been debated for a long time (Poulsen et al., 2001; Donnadieu et al., 2006; Fluteau et al., 2007). Recent model results of higher complexity and higher resolution support only a weak impact of Cretaceous paleogeographic changes on global temperature evolution (Lunt et al., 2016; Tabor et al., 2016). In contrast, first order controls on temperature from changes in atmospheric CO_2 concentrations have received support from both paleo-CO_2 reconstructions (Fletcher et al., 2008; Wang et al., 2014) and model simulations (Tabor et al., 2016). Indeed, compilations of paleo-CO_2 concentrations across the Cretaceous suggest that CO_2 and temperatures broadly increased to peak levels during the Cenomanian and Turonian thermal maximum, before decreasing throughout the Late Cretaceous (Wang et al., 2014). The comparison between model simulations at different plausible Cretaceous CO_2 levels and proxy reconstructions of sea surface temperatures (SST) provides further support to a Late Cretaceous cooling trend driven by decreasing CO_2 levels (Tabor et al., 2016).

Late Cretaceous cooling is expressed heterogeneously at a regional scale and reveals inter-basinal variations in both the surface and deep ocean (Friedrich et al., 2012; O'Brien et al., 2017; Huber et al., 2018). For instance, records from the North Atlantic and Indian Ocean show cooling from the Turonian to the mid-Campanian and stabilization or warming afterward, whereas records from the Pacific Ocean and from the Atlantic and Indian sectors of the Southern Ocean show gradual cooling from the Turonian to the Maastrichtian (MacLeod et al., 2005; Huber et al., 2018). These distinct regional trends suggest that the pathways of water masses and connections between ocean basins changed during the Late Cretaceous, as a result of the evolving paleogeography.

https://doi.org/10.5194/cp-2019-157
Preprint. Discussion started: 16 January 2020

This conjecture is corroborated by studies of the neodymium (Nd) isotopes (expressed as ε_{Nd}), which are quasi-conservative tracer of water masses (Piepgras and Wasserburg, 1982; Frank, 2002; Tachikawa et al., 2003), and their trends through time and differences among sites. Records of Nd isotopes illustrate in particular a long-term shift toward more unradiogenic (lower) values in the Atlantic basin between the Turonian and the Campanian (e.g., MacLeod et al., 2011; Martin et al., 2012; Moiroud et al., 2016; Batenburg et al., 2018). However, there is no consensus on the specific modes and evolution of ocean circulation across the Late Cretaceous, partly due to the lack of Late Cretaceous ε_{Nd} records in key places and times and possible modification of values along flow paths. In addition, deep-water formation during the Late Cretaceous has been hypothesized to occur (alternatively or concurrently) in most high-latitudes basins, including the South Atlantic and Indian Ocean (e.g., Robinson et al., 2010; Murphy and Thomas, 2012; Robinson and Vance, 2012), North Atlantic (e.g., MacLeod et al., 2011; Martin et al., 2012), North Pacific (e.g., Hague et al., 2012; Thomas et al., 2014; Dameron et al., 2017) and South Pacific (e.g., Thomas et al., 2014; Dameron et al., 2017), as well as possibly in the low latitudes (e.g., Friedrich et al., 2008; MacLeod et al., 2008; MacLeod et al., 2011).

Numerical models have been instrumental in providing a framework for interpreting the paleoceanographic data and in shedding light on new hypotheses, yet the location of possible sources of deep-water differs between simulations almost as much as it does among proxy studies (e.g., Brady et al., 1998; Poulsen et al., 2001; Otto-Bliesner et al., 2002; Zhou et al., 2008; Monteiro et al., 2012; Donnadieu et al., 2016; Ladant and Donnadieu, 2016; Lunt et al., 2016). Numerous factors may explain this spread, in particular differences in model complexity and resolution and differences in the paleogeography employed, which may vary across model studies (Donnadieu et al., 2016; Lunt et al., 2016; Tabor et al., 2016). Even within identical Cretaceous time slices, there can be significant differences in paleogeographic reconstructions resulting in additional uncertainty regarding the areas of deep-water formation as well as the configuration of oceanic gateways, and thereby the modes of ocean circulation (e.g., Donnadieu et al., 2016; Lunt et al., 2016; Farnsworth et al., 2019). The considerable impact of breaching a continental barrier or closing an oceanic seaway has indeed long been demonstrated in idealized and paleoclimatic model studies (e.g., Toggweiler and Samuels, 1995;

https://doi.org/10.5194/cp-2019-157
Preprint. Discussion started: 16 January 2020

Climate of the Past
Discussions

Poulsen et al., 2003; Sijp and England, 2004; Sepulchre et al., 2014; Donnadieu et al., 2016; Elsworth et al., 2017; Ladant et al., 2018; Tabor et al., 2019).

Inter-basinal differences in temperature evolution and shifts in the global ocean circulation therefore point toward a critical role of paleogeographic reorganizations, such as the geometry of oceanic basins or the opening, closure and depth changes of oceanic gateways, regardless of the evolution of atmospheric CO_2 during the Late Cretaceous. To our knowledge, only one coupled ocean-atmosphere model study focused on the evolution of global ocean circulation during the Late Cretaceous (Donnadieu et al., 2016). Using Cenomanian-Turonian and Maastrichtian simulations, Donnadieu et al. (2016) demonstrated a shift toward a more vigorous ocean circulation in the Atlantic through time with a shift from South Pacific to South Atlantic and Indian Ocean deep-water source areas. These changes are associated with a reversal of deep-water fluxes across the Caribbean Seaway between North and South America, which provides a possible explanation for decreasing ε_{Nd} values throughout the Atlantic during the Late Cretaceous (Donnadieu et al., 2016). They further suggested that the paleogeographic evolution of the Late Cretaceous was instrumental in preventing later occurrences of OAEs (Donnadieu et al., 2016).

In this contribution, we use a recent and higher resolution earth system model than used in the Donnadieu et al. (2016) study to perform Cenomanian and Maastrichtian simulations as well as a number of sensitivity experiments to evaluate the effect of changes in the depth of major Maastrichtian gateways including the Labrador Seaway, Drake Passage, Caribbean Seaway and Tethys Seaway. The paper is organized as follows: First, we briefly review the paleogeographic history of major Late Cretaceous gateways to describe the rationale behind prescribed gateway changes. We then explore the evolution of the global ocean circulation in the Late Cretaceous with a particular focus on the changes in intermediate and deep-water currents across the globe. Finally, we compare our simulated ocean circulation with compilations of geochemical data in order to provide an updated picture of the global ocean circulation at the close of the Mesozoic era.

https://doi.org/10.5194/cp-2019-157
Preprint. Discussion started: 16 January 2020

Paleogeographic considerations

Previous observational and model examinations of Late Cretaceous ocean circulation changes suggested several plausible explanations for the geochemical record. Advances in the knowledge of the geological history of ocean gateways, combined with modeling of the likely effects of those changes, may provide critical arguments in favor of some modes of Late Cretaceous ocean circulation over others. This section summarizes observations on Late Cretaceous paleogeography in critical regions relative to the Cenomanian (~ 95 Ma) and early Maastrichtian (~ 70 Ma) paleogeographic reconstructions used in our model simulations and sensitivity experiments. These two reconstructions are based on proprietary paleogeographies provided by Getech Plc (Fig. 1), which have been introduced by Lunt et al. (2016).

1. Equatorial Atlantic

Rifting between western Africa and eastern Brazil began during the Early Cretaceous (Mascle et al., 1988). Marine waters invaded this narrow corridor from both ends during the Early Aptian and a shallow marine connection between the Central and South Atlantic oceans exist around 104 Ma (Brownfield and Charpentier, 2006; Ye et al., 2017). The NE-SW motion of the South American plate relative to the African plate is accommodated across transform-related marginal ridges dividing the Equatorial Atlantic Ocean into narrow basins during Albian-Cenomanian (Basile et al., 2005; Jones et al., 2007), which restrict seawater exchanges between the Central and South Atlantic oceans and favor euxinic conditions and black shales deposits in these basins (Pletsch et al., 2001; Ye et al., 2017). Deep-water exchange among basins was still limited from the Turonian to the middle Coniacian (Pletsch et al., 2001), but the disappearance of black shales in the Equatorial Atlantic during the Campanian suggests the initiation of a reliable supply of oxygenated deep water from South Atlantic Ocean at this time (Jones et al., 2007), thereby marking the beginning of a fully opened connection between the Central and South Atlantic oceans.

Our Cenomanian and Maastrichtian paleogeographies (Fig. 1) are consistent with this geological history of the Equatorial Atlantic gateway. In our Cenomanian paleogeography, this

https://doi.org/10.5194/cp-2019-157
Preprint. Discussion started: 16 January 2020

gateway is restricted to a narrow channel with a maximum depth of ~ 2000 m, whereas in the Maastrichtian paleogeography, the Atlantic is opened to full deep-water connection between the North and South Atlantic.

2. Labrador and East Greenland Seaways

Rifting in the Labrador Sea began during the Early Cretaceous, possibly as early as the Valanginian (Dickie et al., 2011), but the onset of sea-floor spreading took place between the Campanian and the Danian (Roest and Srivastava, 1989; Chalmers and Pulvertaft, 2001). This onset is associated with a deepening of the Labrador Sea as indicated by the presence of agglutinated foraminifera from the Maastrichtian onwards (Kuhnt et al., 1989; Setoyama et al., 2017). East of Greenland, the subsidence of the shallow seas occurs later during the Paleocene (Gernigon et al., 2019).

The proto Labrador Sea is closed in our Cenomanian paleogeography (Fig. 1). Although evidence suggests that a proto Labrador Sea potentially existed before the Campanian (Dickie et al., 2011), it would have been restricted to shallow depths with limited influence on interbasinal exchange due to the absence of a northward connection to the Arctic Ocean. The configuration of the proto Labrador Sea in our Maastrichtian paleogeography (Fig. 1) is in line with the distribution of agglutinated foraminifera (Setoyama et al., 2017), with shallow seas East of Greenland and a deeper proto Labrador Sea to the south. However, the exact paleodepth of the Maastrichtian Labrador and East Greenland seas is still poorly constrained. We investigate the possibility of the existence of deeper marine channels in the Maastrichtian northern North Atlantic by deepening the Labrador and East Greenland seas to 4000 m. This sensitivity experiment represents an end-member of the deepest paleogeographic configuration of the northern North Atlantic in the Maastrichtian and we note that a deep East Greenland sea are not supported by Cretaceous geologic evidence.

3. Drake Passage

The history of Drake Passage is intertwined with the evolution of the South America–Antarctic Peninsula–Scotia plate system (Eagles, 2016). The geometrical arrangement of southern

https://doi.org/10.5194/cp-2019-157
Preprint. Discussion started: 16 January 2020

South America and the Antarctica Peninsula (AP) has been a matter of debate since the pioneering work of Wegener (1924). Paleomagnetic inclinations measured in rocks from the Fuegian Andes have been shown to be statistically indistinguishable from those of the Antarctica Peninsula for the Late Cretaceous (Poblete et al., 2016), suggesting that the tip of the AP remained close to Tierra del Fuego. In addition, rocks from the Navarino microplate (Fuegian Andes) recorded a 100° counterclockwise rotation over the last 120 Myr, which suggests that the AP and the southern Andes formed a linear and continuous margin during the Early Cretaceous (Poblete et al., 2016). Likewise, a clockwise rotation was found in the apparent polar wander path of the AP coeval with the rotation of the Navarino microplate, thus confirming the oroclinal bending of the Fuegian Andes (Milanese et al., 2019). During the Cenomanian the oroclinal bending is at an early stage, such that the tip of the South American plate was still connected to the AP, with the possible existence of a land bridge allowing terrestrial and fresh water vertebrate taxa interchange (Poblete et al., 2016). Presence of a land bridge for terrestrial exchange does not exclude the possible existence of seawater connections, but indicates that any connections would have been restricted to shallow water depths. The oroclinal bending continues during the Late Cretaceous but the AP and southernmost South America remain close to each other during the Maastrichtian. This geography is supported by paleontological evidence placing the onset of terrestrial faunistic isolation in South America in the Late Paleocene around 58 Ma (Reguero et al., 2014). The final disruption of the AP-Patagonia system occurred during the Early Eocene but the development of deep-water exchange through the Drake passage only began during the Late Eocene (Scher and Martin, 2006; Lagabrielle et al., 2009). In summary, although the complexity of the South America–Antarctic Peninsula–Scotia plate system's geologic history still hampers comprehensive tectonic reconstructions of the Drake Passage region during the Late Cretaceous, recent evidence indicates that any potential seawater connection would have been restricted to shallow water.

In our Cenomanian paleogeography, the deepest part of the Drake Passage reaches ~ 800 m along a narrow corridor, while in the Maastrichtian, only upper ocean water exchange is possible through the Drake Passage as its deepest part reaches ~ 400 m. Our Cenomanian and Maastrichtian paleogeographic reconstructions are thus broadly consistent with this picture (Fig. 1), although our

Cenomanian Drake Passage might be slightly too deep. However, alternative paleogeographic reconstructions exist, in which the Drake Passage exhibits an even deeper configuration (Sewall et al., 2007; Donnadieu et al., 2016; Niezgodzki et al., 2017). Because the recent study of Donnadieu et al. (2016) documents only minor changes to the global ocean circulation for depths of the Drake Passage lower than 1000 m, we have chosen to prescribe a full deep-ocean connection in order to maximize the potential impact of the deepening of Drake Passage on ocean circulation, even if these abyssal depths are probably exaggerated in the Maastrichtian. The depth of the Drake Passage is thus deepened to 4000 m in our sensitivity experiments (Fig. 1).

4. Caribbean Seaway

The Caribbean region has a complex geological evolution, which started during the Jurassic with the dislocation of Pangaea (Pindell and Kennan, 2009). Rifting between North and South America during the Jurassic and Early Cretaceous led to the opening of the proto-Caribbean seaway. To the west, subduction of the Farallon plate beneath the proto-Caribbean seaway during the Early Cretaceous formed an oceanic volcanic arc stretching from the northwestern tip of South America to the southern tip of North America (Pindell and Kennan, 2009). Emplacement of the Caribbean Large Igneous Province (CLIP) starting in the Cenomanian marked a turning point in the history of the Caribbean region. This large (4 million km^3) basaltic oceanic plateau was formed from 94–89 Ma (Andjić et al., 2019, and references within) or 95–83 Ma (Dürkefälden et al., 2019) by melting during the initial plume head stage of Galapagos hotspot. The CLIP was initially located along the southern edge of the North America plate and the northwestern edge of the South America plate, westward of the oceanic island arc (Andjić et al., 2019). Constructed from 8 – 20 km of thick buoyant basaltic crust emplaced on the oceanic crust of the Farallon plate, the CLIP prevented subduction of the Caribbean plate (Pindell and Kennan, 2009). During the Cenomanian, the CLIP was located in the Caribbean Gateway and its buoyancy restricted exchange to shallow water passages (Buchs et al., 2018), with local subaerial emergence, as indicated by volcaniclastic deposits exposed in the Western Cordillera of Colombia (Buchs et al., 2018). The CLIP then progressively moved eastward relative to the North and South American plates during the Late Cretaceous and new subduction zones were initiated on both

https://doi.org/10.5194/cp-2019-157
Preprint. Discussion started: 16 January 2020

the east and west sides of the CLIP, leading to new volcanic oceanic arcs (Pindell and Kennan, 2009). Paleontological evidence also supports restricted water exchange between the Pacific and the Atlantic during the latest Cretaceous (Iturralde-Vinent, 2006; Ortiz-Jaureguizar and Pascual, 2011). Recent research, therefore, suggests that the Caribbean Gateway was relatively shallow across the Late Cretaceous interval.

Our Cenomanian and Maastrichtian paleogeographies are consistent with these interpretations. The Cenomanian Caribbean Gateway is deeper than that of the Maastrichtian, which is in reasonable agreement with the progressive formation of the CLIP and its eastward motion between the North and South American plates (Buchs et al., 2018). Although geologic evidence does not support the existence of a deep-water connection between the Pacific and the Atlantic in the Late Cretaceous, alternative paleogeographic reconstructions have been employed, in which the Caribbean Seaway is opened to deep flow (Sewall et al., 2007; Donnadieu et al., 2016). As we did for the Drake Passage, we investigate the consequences of prescribing a full deep-ocean connection through the Caribbean Seaway, by deepening the southern portion of this seaway to 4000 m (Fig. 1).

5. Tethys Seaway

The Tethys Ocean exhibits a complex geological history. There is evidence for Late Cretaceous marine exchange between the Central Atlantic Ocean and the Tethys Ocean, which mostly occurred through narrow and deep corridors (Stampfli, 2000; Stampfli and Borel, 2002; Nouri et al., 2016). These corridors formed during the final break-up of the Pangaea supercontinent, which led to the opening of the Alpine Tethys Ocean during the Early Jurassic coeval with the opening of the Central Atlantic Ocean (Stampfli and Borel, 2002). The Alpine Tethys Ocean began to close in the Early Cretaceous in response to the rotations of Africa plate and the Iberian plate (Stampfli and Borel, 2002). During the Late Cretaceous, two deep marine corridors located on both sides of the Anatolides-Taurides permit water exchanges between the Central Atlantic Ocean and the Tethys Ocean (Stampfli and Borel, 2002; Nouri et al., 2016) but it is unclear whether bathymetric sills locally restricted these exchanges to shallow depths (Stampfli and Borel, 2002).

https://doi.org/10.5194/cp-2019-157
Preprint. Discussion started: 16 January 2020

Climate of the Past
Discussions

In our paleogeographic reconstructions, the Cenomanian Tethys Ocean allows a deep-water marine connection through the Tethys, whereas the Maastrichtian Tethys Ocean does not (Fig. 1). The continued convergence of the African and Eurasian plates throughout the Late Cretaceous (Stampfli and Borel, 2002) can be tentatively used to support the existence of deeper connections in the Cenomanian than the Maastrichtian, but existing uncertainties still preclude any firm conclusions on the absence of deep-water connection through the Tethys Ocean in the Maastrichtian. Here, as above, we investigate the consequence of a full deep-ocean connection (4000 m depth) between the Indian Ocean and the North Atlantic.

Models and spinups

The simulations are performed with the CCSM4 earth system model (Gent et al., 2011, and references therein). Our CCSM4 setup is comprised of the POP2 dynamic ocean model, the CAM4 atmosphere model, the CLM4 land surface model and the CICE4 sea ice model. The atmosphere and land-surface components run on a finite-volume grid at 1.9° x 2.5° resolution with 26 uneven vertical levels, while the ocean and sea-ice components run on a rotated pole distorted grid at roughly 1° resolution with 60 vertical levels that vary in thickness with depth.

We perform two baseline simulations of the Cenomanian and early Maastrichtian, which are branched from the 1500-year long CEN and MAA simulations described in Tabor et al. (2016) and respectively run for 500 and 850 additional years with prescribed vegetation fields adapted from Sewall et al. (2007) rather than the dynamic vegetation model of Tabor et al. (2016). Other boundary conditions do not change, such that the atmospheric CO_2 concentration is set to 1120 ppm (4 times the preindustrial value) in line with proxy-based reconstructions (Wang et al., 2014), whereas other greenhouse gas concentrations are set to their preindustrial values. We use a modern Earth orbital configuration and the total incoming solar irradiance is reduced to appropriate Cenomanian and Maastrichtian values of 1353.9 and 1357.18 $W.m^{-2}$ respectively, following Gough (1981).

The gateway sensitivity experiments, in which a single gateway — either the Labrador Seaway, Drake Passage, Caribbean Seaway, or Tethys Seaway — is deepened to 4000 m, are branched from the 850-year long extension of our Maastrichtian simulation. Note that we refer to these bathymetric regions as gateways (or seaways) for simplicity although they may not be gateways in its truest sense (i.e. a narrow passage connecting two otherwise separated ocean basins). The baseline Maastrichtian case and four sensitivity experiments are each run for another 950 years. In total, the Cenomanian and the various Maastrichtian simulations have thus been run for 2000 and 3300 years respectively.

After the 950-year extensions, the simulations reached quasi-equilibrium in the deep ocean, as characterized by timeseries of temperature and meridional overturning circulation (MOC, Fig. 2). A small residual trend exists in the intermediate ocean of the Maastrichtian simulation (1000 m temperatures), which is probably linked to the interval of MOC intensification in this simulation (Fig. 2). This small trend is unlikely to affect the outcomes of this study because the patterns of the ocean circulation do not change during the interval of lower MOC intensity.

Our version of CCSM4 incorporates an ideal age tracer of water masses, which is often used as a tool to track water mass pathways. Ideal age is an ideal tracer in a fully equilibrated ocean. However, for an ocean that is initiated from an unequilibrated state, the ideal age tracer is affected by the spinup history and does not track the equilibrium circulation. To use this tracer, the simulations would require an additional 2000 years of integration, a computational expense that we could not afford. Alternative techniques, such as Newton-Krylov solvers, exist to estimate the equilibrium values of ocean tracers in an offline procedure (e.g., Bardin et al., 2014; Lindsay, 2017) and will be the focus of future work. In this paper, we use the ideal age tracer only as a complementary diagnostic of deep-water formation regions.

Results presented in the following sections are averaged over the last 100 years of each simulation. We first describe general characteristics of the surface climate and of the global overturning circulation, as well as how ocean temperatures respond to changing paleogeography. Next, we focus on the intermediate and deep circulation and analyze how circulation patterns differ between the Cenomanian and the Maastrichtian. To characterize differences, we track the exchange of

https://doi.org/10.5194/cp-2019-157
Preprint. Discussion started: 16 January 2020

Climate of the Past Discussions

water across major oceanic sections by calculating positive and negative water fluxes (Table 1) for three depth ranges—upper ocean (< 500 m depth), intermediate ocean (500 – 1500 m) and deep ocean (> 1500 m). Note that we refer to the net exchange across a section as the sum of positive and negative fluxes across the section. We then put the simulated changes in ocean circulation between the Cenomanian and the Maastrichtian and between the Maastrichtian and the gateway sensitivity experiments into perspective with previous modeling studies and geochemical data.

Results

1. Cenomanian circulation

1.1. Surface climate and global overturning circulation

The global-average annual surface ocean (first 100 m) temperature of the Cenomanian simulation reaches 26.1 °C. Maximum upper ocean temperatures of more than 34 °C are found in the low-latitudes in the western Pacific Ocean and in the Saharan epicontinental sea in Africa, whereas the eastern Pacific Ocean is much cooler because of wind-driven upwelling (Fig. 3A). Relatively warm (> 10 °C) waters exist in the high-latitudes in the Southern Ocean and the North Pacific, though high-latitude coastal and Arctic Ocean waters are colder. Arctic Ocean mean surface ocean temperatures average 2.7 °C. The cold conditions in the Arctic Ocean allow for the formation of winter sea ice (Fig. S1). The Southern Ocean does not freeze seasonally with the exception of an inlet between the Antarctic and Australian continents (Fig. S1).

The modeled upper ocean salinity generally correlates with patterns of precipitation minus evaporation (PME). The highest open ocean salinities are found in subtropical evaporative areas in the center of major ocean gyres while lower values are found in the equatorial Indian Ocean and western Pacific and in the high-latitudes (Fig. 3B and 3C). The Arctic Ocean contains low salinity values reflecting the fact that it is a nearly enclosed basin in a region of net freshwater input. In addition, the spatial distribution of salinity is affected by freshwater input from continental rivers (Fig. 3D), in particular in coastal areas and epicontinental seas. The epicontinental northwestern part of Asia is a region of low salinity due to the isolation of this seaway from the open ocean and of the supply of freshwater from runoff and precipitation. Other low salinity coastal waters include equatorial Africa and South America as well as the isolated basin located between Australia and Antarctica. In contrast, high salinity waters are found in South America, on the Asian margin of the Tethys Ocean and in the Gulf of Mexico (Fig. 3B) and correlate with regions of high temperature, low river freshwater input and largely negative PME (Fig. 3A-D).

The Pacific sector of the Southern Ocean is comparatively warmer and more saline than other high-latitude regions. Cooler and fresher waters in the North Pacific are due to the mixing of North Pacific waters with cold, fresh Arctic waters across the Cenomanian Bering Strait. In the Indo-Atlantic sector of the Southern Ocean, seawater salinities are lower than in the Pacific sector due to the large relative freshwater flux from riverine input into a smaller basin (Table S1). The other major reason for this South Pacific anomaly is a temperature- and salt-advection feedback linked to the winter deepening of the mixed-layer depth (MLD) associated with a large area of deep-water formation (Fig. 3E). The same process occurs in the North Atlantic, albeit at a smaller scale in terms of areal extent and of depth reached by sinking waters (Fig. 3F). Predicted global MOC is essentially fed by sinking South Pacific waters, which drive a strong overturning cell in the Southern Hemisphere, with a maximum of ~ 18 Sv around 40°S and 2000 m, and whose lower limb extends to approximately 40°N at depths of ~ 4000 m (Fig. 4A). In the Northern Hemisphere, the formation of intermediate waters in the North Atlantic leads to a weak Atlantic Meridional Overturning Circulation (Figs. 4A and S2), which reaches up to ~ 1500 – 2000 m around 40°N (Fig. S2).

1.2. Intermediate (500 – 1500 m) circulation

The intermediate ocean circulation is fed primarily by two sources: upwelling of deep waters and sinking of upper ocean waters to intermediate depths (Fig. 3E and 3F). North Atlantic intermediate waters are composed of upper waters that sink in the North Atlantic, upwelled deep waters from the Tethys Ocean advected across the Mediterranean (Table 1, Mediterranean section, and Fig. 5), and weaker inputs of intermediate waters from the Pacific and central Atlantic (Table 1, Caribbean and Central Atlantic sections, and Fig. 5). More than 90% of the intermediate waters advected out of the North Atlantic flow westward across the Caribbean gateway (Table 1, Caribbean

https://doi.org/10.5194/cp-2019-157
Preprint. Discussion started: 16 January 2020

and Central Atlantic sections) while the remaining fraction flows southward through the South Atlantic to the Southern Ocean where it is joined by weak transport of Pacific intermediate waters across Drake Passage (Table 1, South Atlantic and Drake sections, and Fig. 5). The South Atlantic intermediate waters are then advected northeastward through the East Indian section to the Indian Ocean (Fig. S4). These waters eventually flow into the Pacific by joining an Indian Ocean recirculation of Pacific intermediate waters, forming a narrow, intense eastward current that follows the Australian coast (Fig. S4). In contrast, intermediate waters circulating toward the northern Indian and Tethys oceans originate exclusively from Pacific intermediate waters. The Pacific intermediate water system is essentially comprised of a mixture of North Atlantic intermediate waters that flow westward through the Caribbean Seaway, upwelled Pacific deep waters and recirculated Indian Ocean intermediate waters mentioned above.

1.3. Deep (> 1500 m) circulation

The southwest Pacific is the source region for deep waters in our Cenomanian simulation (Fig. 3E). These sinking waters either fill the deep eastern Pacific basin or are advected westward across the Indonesian section, following a strong coastal current around Australia (Figs. 6 and 7). Deep waters crossing the Indonesian section following this westward current mostly recirculates back to the Pacific and mix with the eastern Pacific deep waters to fill the North Pacific basin. Less than 10% of the westward flowing deep waters that have crossed the Indonesian section are advected southward across the East Indian section to the Southern Ocean (Table 1, Indonesian and East Indian sections). Indian sector deep waters exported northward to the Tethys Ocean mostly come from a deep intermediate westward current that follows the southern tip of Asia between ~ 800 and 2400 m (Fig. 7C and Table 1, Indo-Asian and Tethys sections). In the Southern Ocean, deep waters are advected to the South Atlantic but regions of shallow bathymetry (e.g., the Kerguelen Plateau) largely restrict deep-water flow and these waters ultimately well up to shallower depths (Fig. 6). The fate of deep waters flowing northward from the Indian basin is similar. These are advected across the Tethys Ocean to the North Atlantic, where they are upwelled to shallower depths because the Caribbean gateway is closed to deep flow (Fig. 6). An examination of the zonally averaged ideal age values in the Atlantic basin reveals that the deepest-sinking waters in the North Atlantic winter MLD regions reach the deep ocean

https://doi.org/10.5194/cp-2019-157
Preprint. Discussion started: 16 January 2020

Climate of the Past Discussions

(Fig. S5 and 3F). These waters are mostly restricted to the North Atlantic; indeed, only a tiny fraction of North Atlantic deep waters is advected southward into the central Atlantic (Table 1).

In summary, the bathymetric restrictions in the Cenomanian Atlantic, Tethys and Southern Ocean largely confine deep-water circulation to the Pacific and northern Indian Ocean. In contrast, a vigorous intermediate circulation marked by a strong circum-equatorial global current exists, although the restricted Central and South Atlantic basins remain mostly stagnant.

2. Maastrichtian circulation

2.1. Evolution of surface climate and global overturning circulation

The combined changes in paleogeography and solar constant from the Cenomanian to the Maastrichtian lead to a global SST warming of only ~ 0.1 °C, suggesting that changes in paleogeography may cause cooling that compensates for the increasing solar constant (Lunt et al., 2016). Though the global temperature change is minimal, there are substantial regional temperature and salinity changes at the surface (Tabor et al., 2016). Maastrichtian North Pacific surface ocean waters warm significantly because of the closure of the Arctic connection (Fig. 8A and 9A). As a result, the Arctic Ocean becomes more enclosed, cools and freshens (Fig. 8 A-B and 9A-B) because it is a region of net freshwater input (Fig. 8C and 8D). The reduction in the intensity of the circum-equatorial global current (Table 1 and Fig. 9C-D) in the Maastrichtian reduces coastal upwellings of deeper and colder waters on the northern coast of Africa and South America, leading to surface warming of up to a few degrees. The eastern equatorial Pacific warms because of a weaker Walker circulation, which reduces the east-west ocean temperature gradient (Poulsen et al., 1998; Tabor et al., 2016). The PME in the eastern equatorial Pacific increases in the Maastrichtian and leads to lower salinity (Fig. 8B-C and 9B). The opening of the South Atlantic Ocean and Southern Ocean during the Late Cretaceous created a wider basin, which allows for a large subpolar gyre to form (Fig. 9D). This gyre reduces the advection of warm and saline subtropical waters in the Southern Ocean along the eastern coast of Africa (Fig. 9C and 9D), which cool and freshen the Southern Ocean (Fig. 9A and 9B). In addition, the Ekman pumping associated to the subpolar gyre leads to upwelling of deeper and

https://doi.org/10.5194/cp-2019-157
Preprint. Discussion started: 16 January 2020

colder waters to the surface, which contributes to cooling the South Atlantic and southern Indian Oceans. In the northern Indian Ocean, the salinity increase (Fig. 9B) is due to changes in the patterns of surface currents, which limits the northward advection of fresher Indian equatorial waters in the Maastrichtian. Finally, cooling in the North Atlantic and warming in the Pacific sector of the Southern Ocean are related to changes in the MOC (Fig. 4B). In contrast to the Cenomanian, the Maastrichtian North Atlantic does not exhibit deep intermediate water formation (Fig. 8E and 8F). This elimination of proto AMOC weakens the advection of warm and saline subtropical waters into the North Atlantic, leading to surface cooling. Conversely, the intensification of South Pacific deep-water formation drives a more expansive global MOC (Fig. 4B) and is associated to surface warming (Fig. 9A) via reinforcement of the temperature- and salt-advection feedback.

2.2. Temperature changes in the intermediate and deep ocean

The Cenomanian to Maastrichtian paleogeographic evolution, in particular the widening of the Atlantic Ocean, the northward migration of the Indian and Australian subcontinents, and the varying configuration of major gateways, results in a complete reorganization of intermediate and deep ocean circulation (Table 1 and Figs. 5 and 6). This reorganization leads to significant changes in temperatures in the ocean interior in the Maastrichtian relative to the Cenomanian (Fig. 10 and S6). The global temperature change essentially reflects the Pacific signal because of the size of the Pacific basin in both stages (Fig. S3). In the South Pacific Ocean, increased ventilation in the Maastrichtian explains most of the warming signal (Fig. 10B and S6). In the North Pacific, Maastrichtian intermediate water cooling is attributed to restriction to shallow water depths (< 500 m) of flow through the Caribbean Passage, hampering westward advection of North Atlantic waters below the uppermost ocean layers. It is important to note that this restriction is only significant because, in the Cenomanian, North Atlantic intermediate waters are warmer than North Pacific intermediate waters due to deep-water formation occurring in the North Atlantic. In the Maastrichtian, due to the absence of deep-water formation in the North Atlantic, intermediate waters are colder because of reduced ventilation (Fig. 10C and S6) and the geometry of the Caribbean gateway and Tethys Ocean, which isolates the basin from intermediate and deep waters exchange with the Pacific and Indian oceans.

The northward displacement of India and the widening of the Atlantic in the Maastrichtian paleogeography reduce the isolation of the deep South Atlantic, and this basin is invaded by deep flow from the Pacific via the southern Indian Ocean (Table 1, East Indian and South African sections, and Fig. 6) leading to lower temperatures (Fig. 10C and S6). Finally, the Indian basin is mostly warmer in the Maastrichtian than it is during the Cenomanian (Fig. 10D). The small deep ocean warming is explained by advection of warmer deep waters formed in the South Pacific. The larger upper intermediate ocean (centered on ~ 500 m depth) warming is explained by differences in the configuration of the Tethys Ocean. In the Cenomanian simulation, Tethys upper intermediate waters, formed in the late winter when the MLD deepens (Fig. 3F), are advected toward the North Atlantic because the Tethys Ocean is open to intermediate and deep waters (Fig. S7A). The closure of the Tethys Ocean to intermediate and deep waters in the Maastrichtian simulation hampers this advection, and flow of these waters shifts toward the northern Indian Ocean (Fig. S7B). These sinking upper intermediate waters carry a higher temperature and salinity signal into the Indian Ocean, which can be followed on transects across the northern Indian Ocean (Fig. S7C-F), and are responsible for the northern Indian Ocean warming in the Maastrichtian.

2.3. Evolution of the intermediate (500 – 1500 m) circulation

With the restriction of intermediate and deep flow through the Caribbean Seaway and the Tethys Ocean, the sources of intermediate waters in the North Atlantic Ocean are deep waters advected from the South Atlantic that are upwelled in the North Atlantic (Fig. 5) and winter downwelling of upper ocean waters in the northern part of the basin (Fig. 8F). North Atlantic intermediate waters return to the Pacific via the South Atlantic and the southern Indian Ocean (Table 1), following a strong eastward coastal current around the northern tip of Australia (Fig. S8) similar to that existing in the Cenomanian simulation (Fig. S4). In the northern Indian Ocean, intermediate waters are primarily composed of intermediate Pacific waters that flow westward across the Indonesian section between 0 and 10°S (Fig. S8), northern Indian Ocean deep waters that are upwelled to shallower depths (Table 1, Indo-Asian section and Fig. 6), and winter upper ocean waters that were downwelled in the eastern Tethys (Fig. S7B). These northern Indian Ocean intermediate waters flow

https://doi.org/10.5194/cp-2019-157
Preprint. Discussion started: 16 January 2020

eastward into the Pacific following a southward current along the eastern Indian margin and mostly join the strong eastward current circulating around Australia (Fig. S8).

2.4. Evolution of the deep (> 1500 m) circulation

In the Maastrichtian, as in the Cenomanian, deep waters are formed in the South Pacific, mostly in the western part of the basin, and flow northwestward along the Australian coast (Fig. 11). Along the northern continental slope of the Australian margin, deep waters either cross the Indonesian section eastward or recirculate to fill the Pacific basin (Table 1 and Fig. 11). As in the Cenomanian, deep waters advected across the Indonesian section then either fill the southern Indian Ocean (Table 1, East Indian section) or journey northward to recirculate toward the Pacific Ocean or the northern Indian Ocean (Table 1, Indo-Asian section and Fig. 11). Because the connections through the Tethys Ocean are restricted to shallow flow in the Maastrichtian, there is no deep flow across the Tethys Ocean (Table 1, Tethys and Mediterranean sections). In contrast, the opening of the South Atlantic and Southern Ocean allows stronger deep-water flow from the Indian Ocean into the South Atlantic (Table 1, East Indian, West Indian and South African sections), which is then advected northward to the North Atlantic (Table 1, South and Central Atlantic sections) and progressively upwelled to shallower depths.

In the Maastrichtian simulation, the net deep circulation appears to flow in the opposite direction of the intermediate circulation (Figs. 5 and 6). It is also interesting to note that the Maastrichtian circulation is characterized by more intense meridional exchanges (compare Cenomanian and Maastrichtian meridional sections in Table 1, for instance the East Indian, South Atlantic and Central Atlantic sections) whereas the Cenomanian circulation is dominated by zonal flow (Table 1, for instance the Indonesian, Tethys and Caribbean sections).

3. Sensitivity of the Maastrichtian circulation to ocean gateways

As shown above, changes in paleogeography between the Cenomanian and Maastrichtian lead to substantial changes in simulated intermediate and deep ocean circulation. In this section, we analyze the influence of specific gateways on Maastrichtian ocean circulation.

https://doi.org/10.5194/cp-2019-157
Preprint. Discussion started: 16 January 2020

3.1. Deepening of the Labrador Seaway

3.1.1. Temperature changes in the ocean

Deepening the Labrador Seaway only marginally impacts the global ocean circulation. In this experiment and as in the Maastrichtian configuration, deep-water formation takes place in the South Pacific and mostly in the western part of the basin. The maximum winter MLD in both hemispheres is only weakly different from that of the Maastrichtian (Fig. S9A) and the resulting MOC is nearly identical in structure and intensity (Fig. 4C). In the northern North Atlantic and Tethys Ocean, the slight deepening of the maximum winter mixed layers (Fig. S9A) is associated with surface ocean warming, whereas the surface ocean cools south of Greenland (Fig. 12A). There are only minor temperature changes in other oceanic basins or in the ocean interior (Fig. 12A and S10).

The pattern of upper ocean temperature change is linked to the altered bathymetry of the Deep Labrador Seaway experiment, leading to substantial reorganization of upper ocean currents in the northern North Atlantic (Fig. S11). In the Maastrichtian simulation, waters originating from the North Atlantic subtropical latitudes are largely confined south of Greenland because the shallow bathymetry of the seas bathing the east of Greenland and modern Europe (Fig. S11A). An intense southward flow originating from higher Arctic latitudes exist along the eastern margin of Greenland. This flow then circulates southeastward around the southern edge of the Eurasian continent toward the Tethys Ocean. In the Deep Labrador Seaway experiment, the deepening of the seas south and east of Greenland breaks the confinement of North Atlantic subtropical waters south of Greenland, which are instead advected eastward toward the Tethys Ocean along the southern margin of the Eurasian continental landmass (Fig. S11B). This eastward current also blocks the southern penetration of the east Greenland current originating from Arctic latitudes, the intensity of which is also reduced. In summary, warm subtropical waters flow eastward in the Deep Labrador Seaway experiment rather than being confined south of Greenland, which cools the upper ocean there and warms the western part of Europe. In the region east of Greenland, the decrease supply of cold high-latitudes waters leads to warming (Fig. 12A).

3.1.2. Intermediate and deep circulation changes

There are no changes in the direction of intermediate and deep-water transports across major oceanic sections in the Deep Labrador Seaway experiment relative to the Maastrichtian simulation (Figs. 5 and 6). The water fluxes are generally slightly higher, which is probably linked to the slight deepening of the North Atlantic and Tethys Ocean winter MLD and associated slight increase in the vigor of ocean circulation (Fig. S12).

3.2. Deepening of the Drake Passage

3.2.1. Temperature changes in the ocean

Deepening of the Drake Passage has a more significant effect on global ocean circulation than the deepening of the Labrador Seaway. Although deep-water formation still occurs in the South Pacific, the intensity of the MOC decreases (Fig. 4D) because deep-water formation is greatly reduced in the South Pacific, in particular along the eastern edge of Zealandia (Fig. S9B). At the latitudes of the Drake Passage, the MLD increases across the whole South Pacific (Fig. S9B) because of the establishment of a deep-water connection through the Drake Passage, which increases the intensity of the eastward current in the South Pacific. The reduction in the intensity of deep-water formation drives upper ocean temperature cooling in the South Pacific, which is partly carried, albeit weakly, at depth to the Atlantic through the Drake Passage (Figs. 12B and S13). The Atlantic is thus better ventilated because the deep Drake Passage connection allows newly formed, young deep waters to invade the Atlantic (Table 1). In contrast, the North Pacific and northern Indian Oceans are less well ventilated because of lower rates of deep-water formation and a lower advection of deep waters across the Indonesian section (Table 1), associated with a small warming.

3.2.2. Intermediate circulation changes

The intermediate circulation with an open Drake Passage undergoes only a few changes relative to the Maastrichtian. An eastward current develops across Drake Passage and joins the southward flow from the Atlantic Ocean. This increase in the net supply of intermediate waters in the Southern Ocean (Table 1, Drake, South Atlantic and South African sections) drives a reversal of the

https://doi.org/10.5194/cp-2019-157
Preprint. Discussion started: 16 January 2020

intermediate circulation west of India (Table 1, West Indian section, and Fig. 5). This northward water flux enhances the intensity of the intermediate circulation in the northern Indian Ocean (Table 1, Indo-Asian section) but the structure of the circulation does not change (Figs. S8 and S14). The Pacific intermediate circulation is also similar in the Drake Passage experiment as it is in the Maastrichtian simulation.

3.2.3. Deep circulation changes

The deep circulation in the equatorial Indian Ocean and at the Indo-Pacific boundary does not change (Fig. S14), but opening the Drake Passage to deep circulation significantly reduces the flux of deep-water flowing westward across the Indonesian section and into the Indian sector of the Southern Ocean (Table 1 and Fig. 6). This change is balanced by eastward flow across the Drake Passage, which becomes the dominant source of deep waters in the Atlantic sector of the Southern Ocean. In the Indian Ocean, most of the water flow directions are similar to the Maastrichtian simulation except west of India where the net southward deep-water flow stops. In contrast to the Maastrichtian simulation, with deepening of the Drake Passage, deep waters in the South and North Atlantic mostly originate from Pacific waters flowing eastward through the Drake Passage rather than waters from the Indian Ocean.

3.3. Deepening of the Caribbean Seaway

3.3.1. Temperature change in the ocean

Similar to the deepening of the Drake Passage, the opening of the Caribbean Seaway to deep flow causes profound restructuring of the global ocean circulation. Deep-water formation continues to take place in the South Pacific with a reduction in the depth of the winter mixed-layer east of Zealandia relative to the Maastrichtian simulation (Fig. S9C). Consequently, the global MOC is slightly weaker between 2000 and 3000 m (Fig. 4E). The deepening of the Caribbean Seaway leads to cooling of the Atlantic intermediate and deep waters and only minor temperature changes in the Pacific and Indian Oceans relative to the Maastrichtian, whereas it leads to limited and spatially heterogeneous upper ocean temperature changes (Figs. 12C and S15). As in the Deep Drake Passage experiment relative to the Maastrichtian, the Atlantic Ocean is better ventilated in the Deep Caribbean

https://doi.org/10.5194/cp-2019-157
Preprint. Discussion started: 16 January 2020

Seaway experiment than in the Maastrichtian simulation, although intermediate and deep waters invade the Atlantic from the north of the basin rather than from the south.

3.3.2. Intermediate circulation changes

As in the Deep Drake Passage experiment, deepening the Caribbean Seaway does not cause major changes to the modeled global intermediate circulation compared to the Maastrichtian simulation. Changes include the development of weak exchanges of similar magnitude between the Atlantic and the Pacific across the Caribbean Seaway as well as the reversal of the intermediate flow across the West Indian section (Table 1 and Fig. 5). However, the fluxes of water transported by these altered flows are small and the overall structure of the intermediate circulation in the Deep Caribbean Seaway remains similar to that of the Maastrichtian (Table 1 and Fig. 5).

3.3.3. Deep circulation changes

The most salient consequence of the deepening of the Caribbean Seaway on the deep circulation is the reversal of the water fluxes in the Atlantic, from a net northward-dominated flow in the Maastrichtian simulation to a southward-dominated flow in the Deep Caribbean Seaway experiment (Fig. 6) due to the invasion of Pacific deep waters into the Atlantic. In the Southern Ocean, the net transport of water shifts from westward-dominated transport to eastward-dominated transport across the South African section (Table 1 and Fig. 6). As in other Maastrichtian simulations, deep waters formed in the South Pacific flow across the Indonesian section and are either advected into the Indian sector of the Southern Ocean or recirculated to the Pacific (Figs. 11 and S14). However a stronger eastward deep-water flow exists at the southern tip of the Asian continent because of the entrainment created by the opening of the Caribbean Seaway to deep circulation (Table 1, Figs. 6 and S14). This strong current and the reversal of the net transport of deep waters between the Atlantic and Indian sectors of the Southern Ocean induce a reversal of the deep flow west of India (Table 1, West Indian section and Fig. 6). The Southern Ocean is filled with a combination of westward-flowing Indian Ocean deep waters and southward-flowing Atlantic deep waters, which originate from the Pacific and have been advected through the Caribbean Seaway.

3.4. Deepening of the Tethys Seaway

3.4.1. Temperature change in the ocean

In the Maastrichtian and sensitivity simulations described so far, the Tethys Seaway is shallow and inhibits intermediate and deep ocean circulation (Fig. 1). The deepening of the Tethys seaway causes a significant reorganization of the circulation. As in the Deep Drake Passage and Deep Caribbean Seaway simulations, deep-water formation occurs in the South Pacific, although the maximum late winter MLD is reduced relative to the Maastrichtian simulation (Fig. S9D), leading to a slight slowdown of the global MOC (Fig. 4F). Changes in ocean temperatures are minor except in the North Atlantic, Tethys, and northwestern Indian Oceans at intermediate depth (Figs. 12D and S16). At these depths, the eastern Tethys and northern Indian Ocean cool slightly and the western Tethys and North Atlantic warm slightly (Figs. 12D and S16). These changes are due to the opening of intermediate and deep connections between the North Atlantic and Indian Oceans. The warmer and saltier sinking winter upper intermediate waters (~ 500 m depth) in the Tethys Ocean (Fig. S9D) are advected toward the North Atlantic rather than the northern Indian Ocean (Fig. S17), which leads to the observed intermediate temperature signal. It is noteworthy that this reorganization of water currents caused by the deepening of the Tethys Seaway is opposite the reorganization caused by the restriction of the Tethys Seaway that occurs between the Cenomanian and the Maastrichtian (Figs. S7 and S17).

3.4.2. Intermediate circulation changes

In the Deep Tethys Seaway experiment the directions of the net intermediate transports of water across oceanic sections are also similar to that of the Maastrichtian (Table 1 and Fig. 5). The deep Tethys Ocean provides an outlet for North Atlantic intermediate waters across the Mediterranean section, which increases the intermediate water fluxes out of the North Atlantic (Fig. 5). However, part of these eastward flowing intermediate waters recirculate to the North Atlantic, both in the uppermost intermediate ocean (~ 500 m), where they join the westward flowing waters that have downwelled in winter in the eastern Tethys Ocean (Fig. S17), and in the deeper intermediate ocean (Fig. S18). As a consequence, the net intermediate water transport across the Mediterranean section only slightly increases from 0.2 Sv in the Maastrichtian simulation to 0.5 Sv in the Deep Tethys Seaway experiment (Fig. 5). The invasion of the Tethys Ocean with North Atlantic intermediate waters also reduces the

https://doi.org/10.5194/cp-2019-157
Preprint. Discussion started: 16 January 2020

inflow of Pacific intermediate waters in the northern Indian and Tethys Oceans (Table 1, Tethys and Indo-Asian sections and Figs. 5 and S18), which leads to the reversal of the intermediate flow across the eastern West Indian section (Table 1 and Fig. 5). Other net intermediate transports remain in the same direction as in the Maastrichtian simulation.

3.4.3. Deep circulation changes

The main circulation difference caused by the deepening of the Tethys Seaway is a reversal of the deep-water flow direction in the Atlantic basin from northward to southward (Fig. 6). In the equatorial Indian Ocean and Indo-Pacific boundary, deep waters circulation is similar to that in the Maastrichtian simulation (Fig. S14); however, the deep eastward Pacific return flow is reduced (Fig. 6 and Table 1, Indonesian section). This change is because the deepening of the Tethys Seaway opens a deep-water pathway for westward flowing deep waters formed in the South Pacific. These South Pacific deep waters divide between a southwestward component, which flows into the Indian sector of the Southern Ocean (Fig. 6), and a northwestward component, which flows into the Tethys Ocean (Fig. 6). The northwestward deep-water flow across the Tethys Ocean induces a reversal of the deep circulation west of India, from a southward-dominated flow in the Maastrichtian to a northward-dominated flow in the Deep Tethys Seaway experiment (Fig. 6). The Tethyan deep waters then flow into the Atlantic sector of the Southern Ocean via the North Atlantic, which explains the reversal of deep-water flow in this basin. The Southern Ocean is bathed by a combination of deep waters coming from the southern Indian Ocean route and from the Atlantic-Tethys route (Fig. 6).

Discussion

With the exception of the Labrador gateway experiment, each change in gateway profoundly alters the Maastrichtian deep ocean circulation. The deepening of the Drake Passage and Caribbean and Tethys Seaways opens barriers to deep circulation, leading to changes in the intensity of circulation and pathways of deep-water flow. At intermediate depths, gateway changes affect the

https://doi.org/10.5194/cp-2019-157
Preprint. Discussion started: 16 January 2020

origin and intensity of intermediate circulation, but have a lesser effect on the flow pathway within and between basins.

1. Comparison to previous model results

In spite of a number of recent Late Cretaceous modeling studies (Upchurch et al., 2015; Ladant and Donnadieu, 2016; Lunt et al., 2016; Tabor et al., 2016; Niezgodzki et al., 2017; Niezgodzki et al., 2019), to our knowledge only Donnadieu et al. (2016) has investigated changes in ocean circulation from the beginning to the end of the Late Cretaceous. That study uses the FOAM model (Jacob, 1997) to conduct simulations of the Cenomanian/Turonian and Maastrichtian using paleogeographies from Sewall et al. (2007). Donnadieu et al. (2016) (hereafter D16) report that the deep ocean circulation in FOAM is highly sensitive to Late Cretaceous paleogeographic evolution and that these paleogeographic changes are responsible for a shift in the sources of Atlantic deep waters and a reversal of the Atlantic deep-water flow, which provide an explanation for the observed decrease in ε_{Nd} in the Atlantic and Indian Ocean during the Late Cretaceous.

The results of our simulations differ substantially from those of D16 in the locations of deep-water formation and flow pathways. The discrepancies between the simulated ocean circulations in the Cenomanian and Maastrichtian are related to differences in the paleogeography in each simulation employed, in particular in the configuration of oceanic gateways. The Cenomanian simulations of D16 show deep-water formation in the North and South Pacific as well as the South Atlantic. North Atlantic deep waters are sourced from the Pacific and enter the Atlantic through a relatively deep Caribbean Seaway (2000-2500 m, Donnadieu et al., 2016). Deep waters formed in the South Atlantic are mostly advected eastward and northeastward toward the Indian Ocean, with a smaller fraction advected northward (Figs. 2a and 3c in D16). When the Caribbean Seaway is shallowed (94 Ma CAS 560m experiment in D16), the North Atlantic invasion by Pacific deep waters stops and the northward export of deep waters from the South Atlantic increases (Fig. 6e and 7e in D16). In our Cenomanian simulation, in which the depth of the Caribbean Seaway is closer to that of the CAS 560m experiment, North and South Atlantic deep waters originate from the Pacific via Tethyian and southern Indian routes, respectively (Fig. 6).

https://doi.org/10.5194/cp-2019-157
Preprint. Discussion started: 16 January 2020

Climate of the Past
Discussions

The Maastrichtian simulations of D16 exhibit deep-water formation in the North Pacific and in the Atlantic and Indian regions of the Southern Ocean, as well as the cessation of South Pacific deep-water formation that occurred in the Cenomanian. In those simulations, enhanced South Atlantic deep-water formation drives enhanced northward export of deep waters into the North Atlantic, and these deep waters are advected into the Pacific through a deep Caribbean Seaway (Figs. 2b, 3b and 3d in D16). When the Caribbean Seaway is shallowed (71 Ma CAS 560 m experiment in D16), northward export of deep waters into the North Atlantic is drastically reduced, while deep flow into the Indian Ocean is enhanced (Fig. 9e, South Atlantic and East Indian sections in D16). Unlike D16, the Caribbean Seaway in our Maastrichtian paleogeography is shallow and restricts exchange between basins, whereas our Deep Caribbean Seaway has a similar depth to the D16 baseline Maastrichtian experiment. Comparing our Maastrichtian simulation with D16 71 Ma CAS 560m experiment and our Deep Caribbean Seaway experiment with D16 Maastrichtian simulation is therefore more meaningful. In our Maastrichtian simulation, the South and North Atlantic are ventilated by deep waters that form in the South Pacific and flow westward along a pathway through the southern Indian Ocean but the shallow Caribbean and Tethys Seaways confine deep-water in the North Atlantic. In addition, deep-water advection is reversed in the Indian Ocean relative to the D16 CAS 560 m experiment because, in our Maastrichtian simulation, deep waters are formed in the South Pacific rather than the Atlantic and Indian sectors of the Southern Ocean.

The difference in the locations of deep-water formation also explains the reversal of deep-water flow between our Deep Caribbean Seaway experiment and D16 baseline Maastrichtian simulation. In our Deep Caribbean Seaway experiment, deep waters from the Pacific invade the Atlantic through the deep Caribbean Seaway and flow southward into the Southern Ocean, whereas in D16 Maastrichtian simulation deep waters from the Atlantic and Indian sectors of the Southern Ocean flow northward into the North Atlantic and invade the Pacific through the deep Caribbean Seaway. Additional results from sensitivity simulations of D16 show that the deep flow directions are mostly unaffected by changes in the depth of Drake Passage in the Cenomanian and Maastrichtian. Our Deep Drake Passage experiment supports fewer changes in deep flow directions in the Maastrichtian than that of the Deep Caribbean Seaway experiment (Fig. 6), although the provenance of deep waters

https://doi.org/10.5194/cp-2019-157
Preprint. Discussion started: 16 January 2020

Climate of the Past
Discussions

bathing the Atlantic changes substantially from a westward flow through the Indian Ocean to an eastward flow through Drake Passage.

The substantial differences between CESM and FOAM and in the details of the simulations make it difficult to unambiguously explain the substantial changes in the source and circulation of deep waters. In comparison to FOAM, CESM is more complex and has higher spatial resolution. In addition, FOAM and CESM simulations differ in the details of the paleogeographies and initial conditions, which hamper explicit examination of why the two models do not form deep waters in the same locations. However, we speculate that freshwater supply via continental runoff is one of the mechanisms that might lead to these different locations of deep-water formation. In both our Cenomanian and Maastrichtian simulations, the South Pacific is a region of low runoff supply relative to the other sectors of the Southern Ocean (Table 1, Fig. 3D and Fig. S19A-B). In addition, the higher elevation and more extensive meridional span of the Rocky Mountains in our reconstructions (Fig. S19C-D) compared to the Sewall et al. (2007) paleogeography used by D16 (Figs. 4 and 5 of Sewall et al., 2007) blocks the advection of moisture across North America (e.g., Maffre et al., 2018), which contributes to decreased surface salinity and prevents deep-water formation in the North Pacific. Finally the lower resolution of FOAM in the atmosphere (7.5° longitude by 4.5° latitude) smooths the Rocky Mountains even more. As a consequence, the moisture flux out of the North Pacific driven by Northern Hemisphere Westerlies is likely enhanced in D16, leading to increased North Pacific surface salinity and more favorable conditions for deep-water formation.

2. Evolution of intermediate and deep-water circulation during the Late Cretaceous

2.1. Neodymium isotope compilation

The Nd isotopic composition of seawater (i.e. the ratio of $^{143}Nd/^{144}Nd$), expressed as ε_{Nd}, has been used for decades as a tracer of the ocean circulation (Piepgras and Wasserburg, 1982; Frank, 2002; Tachikawa et al., 2003). Seawater ε_{Nd} values are mainly controlled by export of dissolved Nd through continental weathering and fluvial runoff to the ocean (e.g., Frank, 2002; Goldstein and Hemming, 2003; Tachikawa et al., 2017) but mass-balance calculations have shown that additional sources, such as exchange with continental margins (or Boundary Exchange, Lacan and Jeandel,

https://doi.org/10.5194/cp-2019-157
Preprint. Discussion started: 16 January 2020

2005), are required to close the Nd budget (Tachikawa et al., 2003; Lacan and Jeandel, 2005; Arsouze et al., 2007; Rempfer et al., 2011). Because the residence time of Nd in the ocean is shorter than the oceanic mixing time (e.g., Frank, 2002; Tachikawa et al., 2003; Rempfer et al., 2011), the ε_{Nd} composition of water masses reflects their geographical provenance and oceanic pathway (Piepgras and Wasserburg, 1982; Frank, 2002; Goldstein and Hemming, 2003; Moiroud et al., 2016; van de Flierdt et al., 2016) and, as such, can be used as a proxy for past ocean circulation.

A compilation of Cenomanian and Maastrichtian ε_{Nd} values based on the compilation from Moiroud et al. (2016) is shown on Fig. 13 and Tables S2 and S3. The ε_{Nd} values at each site are averaged between 100 Ma and 90 Ma for the Cenomanian and between 75 Ma and 65 Ma for the Maastrichtian. We perform this temporal averaging because the paleogeographies of the Cenomanian and Maastrichtian are not reconstructed with a temporal resolution higher than a few million years. It is thus not possible to attribute a precise age to our Cenomanian (or Maastrichtian) paleogeography, which could equally appropriately represent a 97 Ma or a 92 Ma paleogeography.

The Cenomanian is characterized by Atlantic and southern Indian Ocean ε_{Nd} values that range mainly between ~ –5 to ~ –6 in the intermediate ocean and ~ –6 to ~ –8 in the deep (Fig. 13). Exceptions to this are the anomalously low ε_{Nd} values recorded in the intermediate western equatorial Atlantic (Demerara Rise, MacLeod et al., 2008; MacLeod et al., 2011; Martin et al., 2012) and the high ε_{Nd} signature of ~ –3 of the tropical Pacific (Shatsky Rise), albeit represented by a single data point (Murphy and Thomas, 2012).

From the Cenomanian to the Maastrichtian, ε_{Nd} values generally decrease by ~ 2 to 3 in the Atlantic and southern Indian Oceans, while Pacific Ocean values are ~ –3.5 to –5.5 (Fig. 13). These ε_{Nd} trends have been the focus of numerous hypotheses suggesting the reorganization of ocean circulation through the Late Cretaceous (e.g., Robinson et al., 2010; MacLeod et al., 2011; Martin et al., 2012; Robinson and Vance, 2012; Murphy and Thomas, 2013; Voigt et al., 2013; Donnadieu et al., 2016; Moiroud et al., 2016). It has been suggested that the subsidence of large volcanic provinces, such as the Kerguelen Plateau or Rio Grande Rise, could have lowered the supply of radiogenic material to the Southern Ocean and could have shifted the signature of Maastrichtian deep water masses formed in the South Atlantic (Robinson et al., 2010) or southern Indian Ocean (Murphy and

https://doi.org/10.5194/cp-2019-157
Preprint. Discussion started: 16 January 2020

Thomas, 2012) to lower values, which would then have been exported northward because the deepened central Atlantic in the Maastrichtian would have allowed Southern Ocean deep waters to invade the North Atlantic (Robinson et al., 2010; Murphy and Thomas, 2012). The cessation of Pacific deep-water supply across the Caribbean Seaway in combination with an increased deep-water formation in the Atlantic and Indian sectors of the Southern Ocean has also been proposed (Donnadieu et al., 2016). Alternatively, the initiation of deep-water formation in the North Atlantic and invasion of the Southern Ocean by North Atlantic deep waters flowing across the equatorial Atlantic could explain the ε_{Nd} trends (MacLeod et al., 2011; Martin et al., 2012). All of these hypotheses explain the similarity in deep-water ε_{Nd} values between the North and South Atlantic and the southern Indian Ocean in the Maastrichtian (Fig. 13) by greater communication between the basins (Robinson and Vance, 2012; Murphy and Thomas, 2013; Moiroud et al., 2016) and, therefore, acknowledge the importance of bathymetric barriers, and specifically the opening of the Atlantic and Southern oceans, on the evolution of the ocean circulation during the Late Cretaceous (Voigt et al., 2013; Batenburg et al., 2018). It is, however, noteworthy that the Cenomanian North and South Atlantic and southern Indian Oceans also exhibit similar deep-water ε_{Nd} values (Fig. 13), although the equatorial Atlantic is closed to deep-water circulation in the Cenomanian (e.g., Jones et al., 2007).

2.2. Cenomanian circulation

In contrast to the model simulations of Donnadieu et al. (2016) and the observational hypotheses of Murphy and Thomas (2012, 2013) and Robinson et al. (2010), our Cenomanian simulation produces deep-water formation in the southwest Pacific, along the eastern coast of Australia, rather than in the South Atlantic or southern Indian Ocean (Fig. 3E). However, the deep-water pathway simulated in our Cenomanian simulation, with waters traveling from their source into the southern Indian and South Atlantic Oceans following a strong westward current around the Australian continent, is reasonably consistent with existing ε_{Nd} proxy records. These deep waters would potentially have carried low ε_{Nd} values into the Indian and Atlantic sectors of the Southern Ocean because the ε_{Nd} values of the margins close to the deep-water formation region in our Cenomanian simulation (eastern coast of Australia and Antarctic coast west of the Ross Sea) are

https://doi.org/10.5194/cp-2019-157
Preprint. Discussion started: 16 January 2020

typically between ~ –7 and ~ –20 (Jeandel et al., 2007; Roy et al., 2007). In the South Atlantic and southern Indian Ocean, deep-water ε_{Nd} values may have been modified by the addition of radiogenic contributions from several volcanic provinces that would raise the seawater value. Alternatively, it is possible that bathymetric barriers limited southwest Pacific deep-water advection to the South Atlantic and southern Indian Ocean sufficiently to allow the ε_{Nd} signature of these deep-water to be overprinted by regional ε_{Nd} supply in the Southern Ocean.

South Atlantic and southern Indian Ocean intermediate and deep sites indeed show a relatively large range of ε_{Nd} values (between ~ –5 and ~ –10, Fig. 13) and there is a wide range of possible ε_{Nd} sources with very different ε_{Nd} values, from the unradiogenic African craton and Brazilian shield in the South Atlantic (Jeandel et al., 2007) and Antarctic terranes in the Atlantic and Indian sectors of the Southern Ocean (Roy et al., 2007) to the radiogenic volcanic provinces of Walvis Ridge and Rio Grande Rise (O'Connor and Duncan, 1990; Murphy and Thomas, 2013; Voigt et al., 2013) and large igneous provinces of the Kerguelen Plateau and Rajmahal traps (Mahoney et al., 1995; Coffin et al., 2002). Precisely attributing the contribution of each source, including input of southwest Pacific deep waters, to the South Atlantic and southern Indian Ocean ε_{Nd} values is, therefore, difficult.

Our Cenomanian simulation predicts an inflow of intermediate and deep waters into the North Atlantic from the Tethys and Mediterranean sections (Table 1 and Figs. 5 and 6). These intermediate and deep waters mostly originate from the equatorial and tropical Pacific via an intense eastward current existing between ~ 800 and 2400 m at the southern tip of Asia, which subsequently follows the eastern coast of Africa into the Tethys Ocean and the North Atlantic (Fig. 14A and 7C). Records from the Tethys (Soudry et al., 2006) and Mid-Pacific (Murphy and Thomas, 2012) shows moderate to high ε_{Nd} values (> –6) from the Cenomanian onwards. Soudry et al. (2006) interprets the shift towards higher ε_{Nd} values in the Cenomanian as increased supply of Pacific waters in the Tethys Ocean relative to the Early Cretaceous, as does Pucéat et al. (2005) in reference to the northward Western Europe ε_{Nd} records. The ε_{Nd} records of Soudry et al. (2006) and Pucéat et al. (2005) come from neritic (shallow) sites and, thus, cannot directly be interpreted as evidence supporting the simulated pathway of intermediate and deep-water masses through the Tethys in our Cenomanian simulation. This pathway, however, provides a possible explanation for the ε_{Nd} signature of the deep North Atlantic (Fig. 13),

https://doi.org/10.5194/cp-2019-157
Preprint. Discussion started: 16 January 2020

Climate of the Past
Discussions

which has more radiogenic values than the nearby North American and North African continents (Jeandel et al., 2007).

This intermediate and deep-water connection between the Pacific and the North Atlantic through the Tethys Ocean is also an alternative scenario to the direct deep-water advection from the Pacific to the North Atlantic through the Caribbean Seaway suggested by Donnadieu et al. (2016), which is problematic given that the Caribbean Seaway was probably closed to intermediate and deep-water flow as early as the Cenomanian (e.g., Buchs et al., 2018). However, alternative hypotheses exist that could explain the ε_{Nd} values of North Atlantic intermediate and deep waters and that we are unable to exclude. In particular, volcanism related to the initial emplacement of the CLIP in the Caribbean Seaway during the Cenomanian could have supplied radiogenic material to the North Atlantic without requiring intermediate and deep-water exchange across the Caribbean Seaway or the Tethys Ocean. This input would raise the ε_{Nd} values of North Atlantic waters and could account for the high ε_{Nd} values (~ –5) observed in Cenomanian samples at Blake Nose in the intermediate North Atlantic (MacLeod et al., 2008). Another possible explanation for Blake Nose and other intermediate North Atlantic ε_{Nd} values could be a local supply of Pacific surface waters in the North Atlantic following a proto-Gulf Stream (Fig. 14B). The radiogenic surface signal could then have been transported to intermediate waters (Fig. 14C) via intermediate water formation in the North Atlantic (Fig. 3 and S5).

As pointed out in many studies, Demerara Rise and Cape Verde ε_{Nd} signatures stand out relative to other intermediate and deep sites (MacLeod et al., 2008; Jiménez Berrocoso et al., 2010; MacLeod et al., 2011; Martin et al., 2012). As in the simulation of Donnadieu et al. (2016), our Cenomanian simulation does not produce low latitude intermediate to deep-water formation at Demerara Rise, as has been suggested by previous work (Friedrich et al., 2008; MacLeod et al., 2008; MacLeod et al., 2011; Martin et al., 2012). It does, however, show that Demerara Rise is bathed by a mixture of intermediate waters formed in the North Atlantic and originating from the Tethys Ocean, while the deeper Cape Verde site is mostly influenced by deeper waters from the Tethys (Fig. 13C). It has been suggested that the low ε_{Nd} values at Demerara Rise could be due to boundary exchange with detrital material with extremely unradiogenic signature from the nearby Guyana shield (Donnadieu et

https://doi.org/10.5194/cp-2019-157
Preprint. Discussion started: 16 January 2020

al., 2016), possibly in conjunction with very restricted local circulation (Moiroud et al., 2016). In the absence of an alternative scenario, we support this interpretation to explain Demerara Rise values and also follow the suggestion that Cape Verde basin values could be driven by local boundary exchange close to the western African craton (Moiroud et al., 2016). We note that this conclusion is consistent with the results of Tachikawa et al. (1999; 2003), which report more unradiogenic values closer to the African continent at a site located in the high organic flux Mauritanian upwelling region rather than at a site located farther from the coast, which suggests a significant influence of boundary exchange processes in this region (Tachikawa et al., 2003).

2.3. Late Cretaceous circulation changes

The opening of the Atlantic and Southern Oceans in our Maastrichtian simulations leads to an increased exchange of intermediate and deep waters between ocean basins (Figs. 5 and 6), in line with previous model simulations (Donnadieu et al., 2016) and proxy-based evidence (e.g., MacLeod et al., 2011; Friedrich et al., 2012; Martin et al., 2012; Murphy and Thomas, 2013; Huber et al., 2018).

The evolution of the ocean circulation between the Cenomanian and the baseline Maastrichtian or Deep Labrador Seaway experiments is reasonably consistent with the ε_{Nd} evolution to lower values. Because the Deep Labrador Seaway circulation is nearly identical to that of the baseline Maastrichtian experiment, we focus on the Maastrichtian simulation. This simulation estimates higher rates of deep waters export from the southwest Pacific to the Indian and Atlantic sectors of the Southern Ocean than the Cenomanian simulation (Fig. 6). The absence of major changes in the provenance of deep currents between our Cenomanian and Maastrichtian model runs in the southern Indian and South Atlantic Oceans suggests that the main cause of the observed decrease in ε_{Nd} in these basins might have been higher inputs of unradiogenic deep waters into the southern Indian and South Atlantic Oceans driven by higher deep-water export rates and, therefore, less time for reactions with more radiogenic sediments (e.g., Haynes et al., in review). Alternatively, the observed ε_{Nd} trend might be caused by the progressive subsidence of large igneous provinces, such as the Kerguelen Plateau, reducing the supply of radiogenic volcanic material to the Southern Ocean (Murphy and Thomas, 2013), but these two hypotheses are not mutually exclusive and are difficult to test.

https://doi.org/10.5194/cp-2019-157
Preprint. Discussion started: 16 January 2020

In our Maastrichtian simulation, northward-flowing deep waters from the Southern Ocean dominate the Atlantic and could, therefore, advect low ε_{Nd} values to the North Atlantic and explain the observed ε_{Nd} signature shift in this basin (Figs. 6 and 13). This idea is consistent with previous arguments for the onset of an input of southern water masses into the North Atlantic (Robinson et al., 2010; Robinson and Vance, 2012; Murphy and Thomas, 2013) but is difficult to reconcile with some details of ε_{Nd} values within the South Atlantic (Voigt et al., 2013; Batenburg et al., 2018), which suggest instead restricted deep circulation until the Paleogene. Other studies have suggested that intermediate and deep waters could be sourced from the North Atlantic (MacLeod et al., 2011; Martin et al., 2012) or from low-latitudes (Friedrich et al., 2008; MacLeod et al., 2008; MacLeod et al., 2011) but the absence of deep-water formation in the North Atlantic or low-latitudes in our Maastrichtian simulation and in recent coupled climate model simulations of the Late Cretaceous (Donnadieu et al., 2016; Lunt et al., 2016; Niezgodzki et al., 2017; Farnsworth et al., 2019; Niezgodzki et al., 2019) is not consistent with a North Atlantic source for deep waters. However, Cenozoic North Atlantic deep-water formation has been shown to be sensitive to details of North Atlantic configuration and bathymetry (Stärz et al., 2017; Vahlenkamp et al., 2018; Hutchinson et al., 2019). It is, therefore, possible that existing Late Cretaceous paleogeographic reconstructions are not sufficiently detailed to allow onset of North Atlantic deep-water production but the simulated pathway of deep waters in our Maastrichtian simulation is more consistent with the input of Southern Ocean waters in the North Atlantic (e.g., Robinson et al., 2010).

The Deep Caribbean Seaway and Deep Drake Passage simulations produce Pacific intermediate and deep waters that invade the Atlantic Ocean via northern or southern routes, respectively (Figs. 5 and 6). This increased supply of Pacific waters into the Atlantic would be expected to increase the ε_{Nd} signature of the Atlantic basin, which is at odds with the observed ε_{Nd} decrease by ~ 2 to 3 units. Our simulations, therefore, argue against the presence of these deep gateways during the latest Cretaceous, in agreement with recent progress in the understanding of the geological history of these gateways but in notable contrast to the simulations of Donnadieu et al. (2016).

https://doi.org/10.5194/cp-2019-157
Preprint. Discussion started: 16 January 2020

In the Deep Tethys simulation, high rates of deep waters are also exported from the southwest Pacific to the Indian sector of the Southern Ocean, which, in conjunction with the subsidence of volcanic provinces could explain the ε_{Nd} decrease in this basin. Because the Tethys Ocean is open to intermediate and deep circulation in this experiment, the deep North Atlantic is filled with westward flowing deep waters from the Indian Ocean, which then flow southward into the South Atlantic. These deep waters are composed of a mixture of southwest Pacific deep waters with low ε_{Nd} values traveling across the southern Indian Ocean and of deep waters that have circulated in the Pacific Ocean, thereby evolving to higher ε_{Nd} values (Haynes et al., in review), before flowing into the northern Indian Ocean following the southern tip of Asia between ~ 2000 and 3000 m (Fig. 15 and S14, Deep Tethys Indonesian section). The low ε_{Nd} values observed in the Maastrichtian Atlantic could be consistent with a Deep Tethys Seaway scenario if deep waters flowing into the North Atlantic were composed of a greater proportion of Pacific deep waters that traveled along the southern Indian Ocean and retained lower ε_{Nd} values than Pacific deep waters that traveled along the northern Indian Ocean and acquired higher ε_{Nd} values. However, this hypothesis is conceptually less elegant and more complicated than the invasion of the North Atlantic by deep waters from the Southern Ocean with low ε_{Nd} values into the North Atlantic, as suggested by our Maastrichtian (and Deep Labrador Seaway) simulation. In addition, the Deep Tethys Seaway hypothesis is not easily reconciled with the geological context of a progressively resorbing Tethys Ocean during the Late Cretaceous (Stampfli, 2000).

It is noteworthy that our Maastrichtian simulations offer no better solution to the low ε_{Nd} signature of Demerara Rise and Cape Verde records (MacLeod et al., 2008; Jiménez Berrocoso et al., 2010; MacLeod et al., 2011; Martin et al., 2012) than local boundary exchange processes within restricted basins (Donnadieu et al., 2016; Moiroud et al., 2016; Batenburg et al., 2018), at least until the extreme end of the Maastrichtian when a convergence of Demerara Rise and other North Atlantic sites ε_{Nd} values is observed (MacLeod et al., 2011). Likewise, our simulations do not provide a particular solution to the high ε_{Nd} values recorded at Site 1276 in the Maastrichtian North Atlantic (Fig. 13). We can only concur that local processes involving more radiogenic material might contribute to this signal (Robinson and Vance, 2012), possibly as early as the Cenomanian (Fig. 13).

https://doi.org/10.5194/cp-2019-157
Preprint. Discussion started: 16 January 2020

2.4. Oxygen and carbon isotopes

Geochemical records of $\delta^{18}O$ and $\delta^{13}C$ have also been employed to reconstruct Late Cretaceous climate and ocean circulation changes. Multi-basin compilations show a global increase in planktic and benthic $\delta^{18}O$ from the Cenomanian-Turonian to the Maastrichtian (Friedrich et al., 2012; O'Brien et al., 2017; Huber et al., 2018), and a progressive reduction in the vertical $\delta^{13}C$ gradient between surface and deep records (Huber et al., 2018). In addition, benthic $\delta^{18}O$ and $\delta^{13}C$ from the major ocean basins progressively converge through the Late Cretaceous (Huber et al., 2018), a trend that has been interpreted to reflect enhanced connectivity between deep ocean basins and that is captured in our simulations.

The comparison between the proxy-based and simulated temperature changes in the surface and deep ocean between the Cenomanian and the Maastrichtian is more complicated. For example, the ~ 1 to 1.5 ‰ positive benthic $\delta^{18}O$ trend observed at Blake Nose (Huber et al., 2002; Huber et al., 2018) could in part be explained by the ~ 2 to 2.5 °C cooling predicted by our model in the North Atlantic (Fig. 10 and S6) between the Cenomanian and the Maastrichtian, but the parallel positive planktic $\delta^{18}O$ trend is not reproduced in our simulations (Fig. 9A). Similarly, in contrast to proxy observations, our model does not predict any significant temperature change at Exmouth Plateau in the southern Indian Ocean or in the deep equatorial Pacific (Ando et al., 2013; Falzoni et al., 2016). In the Atlantic sector of the Southern Ocean, our model predicts a small cooling, which is consistent with the $\delta^{18}O$ proxy record in terms of direction of change but falls short of explaining the amplitude of change (Huber et al., 2018).

A likely cause for this disagreement is that our simulations were performed with a constant atmospheric CO_2 concentration of 1120 ppm in order to isolate the impact of changing paleogeography on the ocean circulation. Proxy evidence indicates that atmospheric CO_2 declined during the Late Cretaceous (e.g., Breecker et al., 2010; Linnert et al., 2014; Wang et al., 2014), although the exact pCO_2 evolution and range remains uncertain (Wang et al., 2014; Foster et al., 2017), and recent model investigations of the Late Cretaceous cooling trend (including with the CCSM4 earth system model, Tabor et al., 2016) have identified CO_2 as the primary driver of this trend (Lunt et al., 2016; Tabor et al., 2016). In addition, CO_2-induced cooling may play a role in explaining

https://doi.org/10.5194/cp-2019-157
Preprint. Discussion started: 16 January 2020

the Cenomanian to Maastrichtian decrease in vertical $\delta^{13}C$ gradients (Huber et al., 2018) because the temperature dependence of metabolic rates in ocean planktonic communities may have increased surface to deep $\delta^{13}C$ gradient in warmer climates (John et al., 2013), by promoting increased rates of primary productivity, thereby enhancing surface $\delta^{13}C$ values, and/or increased remineralization of organic matter, which would enhance the ^{13}C depletion in the ocean interior.

Part of the mismatch between simulated temperature changes and $\delta^{18}O$ records may also pertain to the fact that foraminiferal $\delta^{18}O$ is a proxy for temperature and seawater $\delta^{18}O$. Foraminiferal $\delta^{18}O$ values are generally converted to temperatures using the consensus value of –1 ‰ for mean ice-free seawater $\delta^{18}O$ (Shackleton and Kennett, 1975; Pearson, 2012). If significant polar ice sheets developed during the Late Cretaceous, which is unlikely during the Cenomanian based on recent observational and model studies (e.g., MacLeod et al., 2013; Ladant and Donnadieu, 2016) but is more debated for the cooler climates of the Maastrichtian (e.g., Miller et al., 1999; Bowman et al., 2013; Ladant and Donnadieu, 2016; Huber et al., 2018), mean seawater $\delta^{18}O$ may have shifted toward higher values. A positive shift in seawater $\delta^{18}O$ would have reduced the magnitude of seawater cooling required to explain the increasing values in foraminiferal $\delta^{18}O$ through the Maastrichtian. However, latest reviews suggest that, in the absence of direct evidence for ice sheet and synchronicity between indirect evidence, Cretaceous ice sheets might only, if ever, have existed as small ice sheets with limited impact on seawater $\delta^{18}O$ (Huber et al., 2018). In contrast, regional deviations from the global mean seawater $\delta^{18}O$ may exert a stronger control on the conversion of foraminiferal $\delta^{18}O$ values to ocean temperatures, in particular in the upper ocean. The mid-Cretaceous simulations of Zhou et al. (2008) with the GENESIS-MOM coupled model indeed indicate significant surface variability in seawater $\delta^{18}O$ in spite of the absence of a river routing scheme. Because precipitations and runoff are depleted in $\delta^{18}O$ relative to seawater, the upper ocean could exhibit more depleted seawater $\delta^{18}O$ in regions of high precipitation and/or high runoff input, with a substantial impact on reconstructed ocean temperatures (Huber et al., 2018).

In summary, the comparison of simulated temperature changes and foraminiferal $\delta^{18}O$ between the Cenomanian and Maastrichtian does not provide strong evidence for or against proposed changes in ocean circulation patterns or the nature of ocean gateways.

https://doi.org/10.5194/cp-2019-157
Preprint. Discussion started: 16 January 2020

Climate of the Past Discussions

Conclusion

Our CCSM4 earth system model simulations of the Cenomanian and Maastrichtian demonstrate significant reorganizations of the deep and intermediate ocean circulation during the Late Cretaceous, which are predominantly controlled by the configuration of major oceanic gateways. Our model predicts continuous deep-water formation in the southwest Pacific in the Late Cretaceous but show that the Cenomanian to Maastrichtian interval witnessed the transition from an essentially zonal ocean circulation to one promoting increased meridional water exchanges. We show that the simulated ocean circulation compares reasonably well to global ε_{Nd} records and that the Caribbean Seaway and Drake Passage were likely restricted to shallow circulation in the Maastrichtian, in agreement with current paleobathymetric knowledge (e.g., Buchs et al., 2018). In contrast, our simulations cannot discriminate whether deep connections existed across the Tethys Ocean on the basis of the comparison with ε_{Nd} records.

We acknowledge however that we are limited in our interpretation of the ε_{Nd} records for several reasons. First, paleogeographic uncertainties require that we average ε_{Nd} values over long time intervals. We are therefore bound to miss higher frequency climatic and oceanic variability, which might explain local ε_{Nd} signatures. Second, most of the neodymium signatures are between ~ -5 and ~ -10, which are relatively "middle-of-the-road" values and represent a large number of plausible sources. The interpretation of local ε_{Nd} values from our model simulations is less certain, whereas we are more confident in interpreting large basin-scale trends (such as the Atlantic and Indian Oceans ε_{Nd} decrease between the Cenomanian and Maastrichtian). Third, there is a real need for increased Cretaceous ε_{Nd} records in particular from the south(west) Pacific and from what remains of the Cretaceous Indian Ocean, regions which are critically under sampled. Fourth, the comparison between ε_{Nd} records and oceanic currents is a step forward to understanding the ocean circulation of the Late Cretaceous and next advances in the latter will probably require specific modeling of the water mass signature in ε_{Nd} (Arsouze et al., 2007; Sepulchre et al., 2014; Gu et al., 2019).

https://doi.org/10.5194/cp-2019-157
Preprint. Discussion started: 16 January 2020

Climate of the Past Discussions

Ultimately, our work highlights the critical impact of gateway configurations in the Late Cretaceous oceanic evolution. The geologic history of major ocean gateways and the continuous deep-water formation in the South Pacific in our simulations suggest that the Late Cretaceous trend in ε_{Nd} values in the Atlantic and southern Indian Oceans was caused by subsidence of volcanic provinces and opening of the Atlantic and Southern Oceans rather than changes in deep-water formation areas and/or reversal of deep-water fluxes. However, other plausible scenarios consistent with Late Cretaceous ε_{Nd} values remain and new studies combining proxy records, detailed paleogeographic reconstructions and ε_{Nd} modeling will therefore be key to improving our understanding of Late Cretaceous climates.

Data availability

All model outputs and scripts for reproducing this work are archived at the University of Michigan or NCAR Cheyenne supercomputer and Campaign storage space. They are available upon reasonable request to jbladant@umich.edu.

Author contributions

JBL performed the model simulations with the help of CJP and CRT and the model analyses. FF reviewed the paleogeographic history of ocean gateways. All authors contributed to discussing and interpreting the results and writing the paper.

Competing interests

The authors declare that they have no conflict of interest.

https://doi.org/10.5194/cp-2019-157
Preprint. Discussion started: 16 January 2020

Climate of the Past
Discussions

Acknowledgments

We acknowledge high-performance computing support from Cheyenne (*doi:10.5065/D6RX99HX*) provided by NCAR's Computational and Information Systems Laboratory, sponsored by the National Science Foundation. We thank Andrew Vande Guchte for the initial setup of the simulations on the NCAR Cheyenne supercomputer. J.-B. Ladant thanks the Institut de Physique du Globe de Paris for permission to use its premises. This work was supported by NCAR/CISL allocation UMIC0063 to J.-B. Ladant and C. J. Poulsen, Heising-Simons Foundation Grant #2016-05 to C. J. Poulsen, and U.S. National Science Foundation (OCE-1261562) to K. G. MacLeod, E. E. Martin, and C. J. Poulsen.

References

Andjić, G., Baumgartner, P. O., and Baumgartner-Mora, C.: Collision of the Caribbean Large Igneous Province with the Americas: Earliest evidence from the forearc of Costa Rica, Geological Society of America Bulletin, 2019.

Ando, A., Woodard, S. C., Evans, H. F., Littler, K., Herrmann, S., MacLeod, K. G., Kim, S., Khim, B. K., Robinson, S. A., and Huber, B. T.: An emerging palaeoceanographic 'missing link': multidisciplinary study of rarely recovered parts of deep-sea Santonian–Campanian transition from Shatsky Rise, Journal of the Geological Society, 170, 381-384, 2013.

Arsouze, T., Dutay, J. C., Lacan, F., and Jeandel, C.: Modeling the neodymium isotopic composition with a global ocean circulation model, Chemical Geology, 239, 165-177, 2007.

Bardin, A., Primeau, F., and Lindsay, K.: An offline implicit solver for simulating prebomb radiocarbon, Ocean Modelling, 73, 45-58, 2014.

Barron, E. J., and Washington, W. M.: Cretaceous climate: a comparison of atmospheric simulations with the geologic record, Palaeogeography, Palaeoclimatology, Palaeoecology, 40, 103-133, 1982.

Barron, E. J.: A warm, equable Cretaceous: the nature of the problem, Earth-Science Reviews, 19, 305-338, 1983.

Barron, E. J., and Washington, W. M.: The role of geographic variables in explaining paleoclimates: Results from Cretaceous climate model sensitivity studies, Journal of Geophysical Research: Atmospheres (1984–2012), 89, 1267-1279, 1984.

Barron, E. J., and Washington, W. M.: Warm Cretaceous climates: High atmospheric CO_2 as a plausible mechanism, The Carbon Cycle and Atmospheric CO: Natural Variations Archean to Present, 546-553, 1985.

Basile, C., Mascle, J., and Guiraud, R.: Phanerozoic geological evolution of the Equatorial Atlantic domain, Journal of African Earth Sciences, 43, 275-282, 2005.

https://doi.org/10.5194/cp-2019-157
Preprint. Discussion started: 16 January 2020

Climate of the Past
Discussions

Batenburg, S. J., Voigt, S., Friedrich, O., Osborne, A. H., Bornemann, A., Klein, T., Pérez-Díaz, L., and Frank, M.: Major intensification of Atlantic overturning circulation at the onset of Paleogene greenhouse warmth, Nature communications, 9, 4954, 2018.

Bowman, V. C., Francis, J. E., and Riding, J. B.: Late Cretaceous winter sea ice in Antarctica?, Geology, 41, 1227-1230, 10.1130/g34891.1, 2013.

Bowman, V. C., Francis, J. E., Askin, R. A., Riding, J. B., and Swindles, G. T.: Latest Cretaceous–earliest Paleogene vegetation and climate change at the high southern latitudes: palynological evidence from Seymour Island, Antarctic Peninsula, Palaeogeography, Palaeoclimatology, Palaeoecology, 408, 26-47, 10.1016/j.palaeo.2014.04.018, 2014.

Brady, E. C., DeConto, R. M., and Thompson, S. L.: Deep water formation and poleward ocean heat transport in the warm climate extreme of the Cretaceous (80 Ma), Geophysical Research Letters, 25, 4205-4208, 1998.

Breecker, D. O., Sharp, Z. D., and McFadden, L. D.: Atmospheric CO2 concentrations during ancient greenhouse climates were similar to those predicted for A.D. 2100, Proceedings of the National Academy of Sciences of the United States of America, 107, 576-580, 10.1073/pnas.0902323106, 2010.

Brownfield, M. E., and Charpentier, R. R.: Geology and total petroleum systems of the Gulf of Guinea Province of West Africa, US Geological Survey, 2006.

Buchs, D. M., Kerr, A. C., Brims, J. C., Zapata-Villada, J. P., Correa-Restrepo, T., and Rodríguez, G.: Evidence for subaerial development of the Caribbean oceanic plateau in the Late Cretaceous and palaeo-environmental implications, Earth and Planetary Science Letters, 499, 62-73, 2018.

Chalmers, J. A., and Pulvertaft, T. C. R.: Development of the continental margins of the Labrador Sea: a review, Geological Society, London, Special Publications, 187, 77-105, 2001.

Coffin, M. F., Pringle, M. S., Duncan, R. A., Gladczenko, T. P., Storey, M., Müller, R. D., and Gahagan, L. A.: Kerguelen hotspot magma output since 130 Ma, Journal of Petrology, 43, 1121-1137, 2002.

Cramer, B. S., Miller, K. G., Barrett, P. J., and Wright, J. D.: Late Cretaceous–Neogene trends in deep ocean temperature and continental ice volume: Reconciling records of benthic foraminiferal geochemistry (δ18O and Mg/Ca) with sea level history, Journal of Geophysical Research, 116, 10.1029/2011jc007255, 2011.

Dameron, S. N., Leckie, R. M., Clark, K., MacLeod, K. G., Thomas, D. J., and Lees, J. A.: Extinction, dissolution, and possible ocean acidification prior to the Cretaceous/Paleogene (K/Pg) boundary in the tropical Pacific, Palaeogeography, palaeoclimatology, palaeoecology, 485, 433-454, 2017.

Davies, A., Kemp, A. E., and Pike, J.: Late Cretaceous seasonal ocean variability from the Arctic, Nature, 460, 254-258, 10.1038/nature08141, 2009.

Dickie, K., Keen, C. E., Williams, G. L., and Dehler, S. A.: Tectonostratigraphic evolution of the Labrador margin, Atlantic Canada, Marine and Petroleum Geology, 28, 1663-1675, 2011.

Donnadieu, Y., Pierrehumbert, R., Jacob, R., and Fluteau, F.: Modelling the primary control of paleogeography on Cretaceous climate, Earth and Planetary Science Letters, 248, 426-437, 10.1016/j.epsl.2006.06.007, 2006.

Donnadieu, Y., Pucéat, E., Moiroud, M., Guillocheau, F., and Deconinck, J.-F.: A better-ventilated ocean triggered by Late Cretaceous changes in continental configuration, Nature communications, 7, 2016.

Dürkefälden, A., Hoernle, K., Hauff, F., Wartho, J.-A., van den Bogaard, P., and Werner, R.: Age and geochemistry of the Beata Ridge: Primary formation during the main phase (~ 89 Ma) of the Caribbean Large Igneous Province, Lithos, 328, 69-87, 2019.

Eagles, G.: Tectonic reconstructions of the Southernmost Andes and the Scotia Sea during the opening of the Drake Passage, in: Geodynamic evolution of the southernmost Andes, Springer, 75-108, 2016.

Elsworth, G., Galbraith, E., Halverson, G., and Yang, S.: Enhanced weathering and CO2 drawdown caused by latest Eocene strengthening of the Atlantic meridional overturning circulation, Nature Geoscience, 10, 213-216, 2017.

Falzoni, F., Petrizzo, M. R., Clarke, L. J., MacLeod, K. G., and Jenkyns, H. C.: Long-term Late Cretaceous oxygen-and carbon-isotope trends and planktonic foraminiferal turnover: A new record from the southern midlatitudes, Bulletin, 128, 1725-1735, 2016.

Farnsworth, A., Lunt, D. J., O'Brien, C. L., Foster, G. L., Inglis, G. N., Markwick, P., Pancost, R. D., and Robinson, S. A.: Climate Sensitivity on Geological Timescales Controlled by Nonlinear Feedbacks and Ocean Circulation, Geophysical Research Letters, 46, 9880-9889, 2019.

Fletcher, B. J., Brentnall, S. J., Anderson, C. W., Berner, R. A., and Beerling, D. J.: Atmospheric carbon dioxide linked with Mesozoic and early Cenozoic climate change, Nature Geoscience, 1, 43-48, 10.1038/ngeo.2007.29, 2008.

Fluteau, F., Ramstein, G., Besse, J., Guiraud, R., and Masse, J. P.: Impacts of palaeogeography and sea level changes on Mid-Cretaceous climate, Palaeogeography, Palaeoclimatology, Palaeoecology, 247, 357-381, 2007.

Foster, G. L., Royer, D. L., and Lunt, D. J.: Future climate forcing potentially without precedent in the last 420 million years, Nature communications, 8, 14845, 2017.

Frank, M.: Radiogenic isotopes: tracers of past ocean circulation and erosional input, Reviews of geophysics, 40, 1-1-1-38, 2002.

Friedrich, O., Erbacher, J., Moriya, K., Wilson, P. A., and Kuhnert, H.: Warm saline intermediate waters in the Cretaceous tropical Atlantic Ocean, Nature Geoscience, 1, 453, 2008.

Friedrich, O., Norris, R. D., and Erbacher, J.: Evolution of middle to Late Cretaceous oceans--A 55 m.y. record of Earth's temperature and carbon cycle, Geology, 40, 107-110, 10.1130/g32701.1, 2012.

Gent, P. R., Danabasoglu, G., Donner, L. J., Holland, M. M., Hunke, E. C., Jayne, S. R., Lawrence, D. M., Neale, R. B., Rasch, P. J., and Vertenstein, M.: The community climate system model version 4, Journal of Climate, 24, 4973-4991, 2011.

Gernigon, L., Franke, D., Geoffroy, L., Schiffer, C., Foulger, G. R., and Stoker, M.: Crustal fragmentation, magmatism, and the diachronous opening of the Norwegian-Greenland Sea, Earth-Science Reviews, 2019.

Goldstein, S. L., and Hemming, S. R.: Long-lived isotopic tracers in oceanography, paleoceanography, and ice-sheet dynamics, Treatise on geochemistry, 6, 625, 2003.

Gough, D. O.: Solar interior structure and luminosity variations, in: Physics of Solar Variations, Springer, 21-34, 1981.

Gu, S., Liu, Z., Jahn, A., Rempfer, J., Zhang, J., and Joos, F.: Modeling Neodymium Isotopes in the Ocean Component of the Community Earth System Model (CESM1), Journal of Advances in Modeling Earth Systems, 11, 624-640, 2019.

Hague, A. M., Thomas, D. J., Huber, M., Korty, R., Woodard, S. C., and Jones, L. B.: Convection of North Pacific deep water during the early Cenozoic, Geology, 40, 527-530, 10.1130/g32886.1, 2012.

Huber, B. T., Norris, R. D., and MacLeod, K. G.: Deep-sea paleotemperature record of extreme warmth during the Cretaceous, Geology, 30, 123, 10.1130/0091-7613(2002)030<0123:dsproe>2.0.co;2, 2002.

https://doi.org/10.5194/cp-2019-157
Preprint. Discussion started: 16 January 2020

Huber, B. T., MacLeod, K. G., Watkins, D. K., and Coffin, M. F.: The rise and fall of the Cretaceous Hot Greenhouse climate, Global and Planetary Change, 167, 1-23, 10.1016/j.gloplacha.2018.04.004, 2018.

Hutchinson, D. K., Coxall, H. K., O′Regan, M., Nilsson, J., Caballero, R., and de Boer, A. M.: Arctic closure as a trigger for Atlantic overturning at the Eocene-Oligocene Transition, Nature communications, 10, 1-9, 2019.

Iturralde-Vinent, M. A.: Meso-Cenozoic Caribbean paleogeography: implications for the historical biogeography of the region, International Geology Review, 48, 791-827, 2006.

Jacob, R.: Low Frequency Variability in a Simulated Atmosphere Ocean System, PhD, University of Wisconsin-Madison, Madison, Wisconsin, USA., 1997.

Jeandel, C., Arsouze, T., Lacan, F., Techine, P., and Dutay, J. C.: Isotopic Nd compositions and concentrations of the lithogenic inputs into the ocean: A compilation, with an emphasis on the margins, Chemical Geology, 239, 156-164, 2007.

Jenkyns, H. C., Forster, A., Schouten, S., and Damsté, J. S. S.: High temperatures in the late Cretaceous Arctic Ocean, Nature, 432, 888-892, 2004.

Jenkyns, H. C.: Geochemistry of oceanic anoxic events, Geochemistry, Geophysics, Geosystems, 11, n/a-n/a, 10.1029/2009gc002788, 2010.

Jiménez Berrocoso, Á., MacLeod, K. G., Martin, E. E., Bourbon, E., Londoño, C. I., and Basak, C.: Nutrient trap for Late Cretaceous organic-rich black shales in the tropical North Atlantic, Geology, 38, 1111-1114, 2010.

John, E. H., Pearson, P. N., Coxall, H. K., Birch, H., Wade, B. S., and Foster, G. L.: Warm ocean processes and carbon cycling in the Eocene, Phil. Trans. R. Soc. A, 371, 20130099, 2013.

Jones, E. J. W., Bigg, G. R., Handoh, I. C., and Spathopoulos, F.: Distribution of deep-sea black shales of Cretaceous age in the eastern Equatorial Atlantic from seismic profiling, Palaeogeography, Palaeoclimatology, Palaeoecology, 248, 233-246, 2007.

Kuhnt, W., Kaminski, M. A., and Moullade, M.: Late Cretaceous deep-water agglutinated foraminiferal assemblages from the North Atlantic and its marginal seas, Geologische Rundschau, 78, 1121-1140, 1989.

Lacan, F., and Jeandel, C.: Neodymium isotopes as a new tool for quantifying exchange fluxes at the continent–ocean interface, Earth and Planetary Science Letters, 232, 245-257, 2005.

Ladant, J. B., and Donnadieu, Y.: Palaeogeographic regulation of glacial events during the Cretaceous supergreenhouse, Nature communications, 7, 12771, 10.1038/ncomms12771, 2016.

Ladant, J. B., Donnadieu, Y., Bopp, L., Lear, C. H., and Wilson, P. A.: Meridional contrasts in productivity changes driven by the opening of Drake Passage, Paleoceanography and Paleoclimatology, 33, 302-317, 2018.

Lagabrielle, Y., Goddéris, Y., Donnadieu, Y., Malavieille, J., and Suarez, M.: The tectonic history of Drake Passage and its possible impacts on global climate, Earth and Planetary Science Letters, 279, 197-211, 10.1016/j.epsl.2008.12.037, 2009.

Lindsay, K.: A newton–krylov solver for fast spin-up of online ocean tracers, Ocean Modelling, 109, 33-43, 2017.

Linnert, C., Robinson, S. A., Lees, J. A., Bown, P. R., Perez-Rodriguez, I., Petrizzo, M. R., Falzoni, F., Littler, K., Arz, J. A., and Russell, E. E.: Evidence for global cooling in the Late Cretaceous, Nature communications, 5, 4194, 10.1038/ncomms5194, 2014.

Lunt, D. J., Farnsworth, A., Loptson, C., Foster, G. L., Markwick, P., O'Brien, C. L., Pancost, R. D., Robinson, S. A., and Wrobel, N.: Palaeogeographic controls on climate and proxy interpretation, Climate of the Past, 12, 1181-1198, 10.5194/cp-12-1181-2016, 2016.

MacLeod, K. G., Huber, B. T., and Isaza-Londoño, C.: North Atlantic warming during global cooling at the end of the Cretaceous, Geology, 33, 437-440, 2005.
MacLeod, K. G., Martin, E. E., and Blair, S. W.: Nd isotopic excursion across Cretaceous ocean anoxic event 2 (Cenomanian-Turonian) in the tropical North Atlantic, Geology, 36, 811-814, 2008.
MacLeod, K. G., Londoño, C. I., Martin, E. E., Berrocoso, Á. J., and Basak, C.: Changes in North Atlantic circulation at the end of the Cretaceous greenhouse interval, Nature Geoscience, 4, 779, 2011.
MacLeod, K. G., Huber, B. T., Berrocoso, A. J., and Wendler, I.: A stable and hot Turonian without glacial d18O excursions is indicated by exquisitely preserved Tanzanian foraminifera, Geology, 41, 1083-1086, 10.1130/g34510.1, 2013.
Maffre, P., Ladant, J.-B., Donnadieu, Y., Sepulchre, P., and Goddéris, Y.: The influence of orography on modern ocean circulation, Climate dynamics, 50, 1277-1289, 2018.
Mahoney, J. J., Jones, W. B., Frey, F. A., Salters, V. J. M., Pyle, D. G., and Davies, H. L.: Geochemical characteristics of lavas from Broken Ridge, the Naturaliste Plateau and southernmost Kerguelen Plateau: Cretaceous plateau volcanism in the southeast Indian Ocean, Chemical Geology, 120, 315-345, 1995.
Martin, E. E., MacLeod, K. G., Berrocoso, A. J., and Bourbon, E.: Water mass circulation on Demerara Rise during the Late Cretaceous based on Nd isotopes, Earth and Planetary Science Letters, 327, 111-120, 2012.
Mascle, J., Blarez, E., and Marinho, M.: The shallow structures of the Guinea and Ivory Coast-Ghana transform margins: their bearing on the Equatorial Atlantic Mesozoic evolution, Tectonophysics, 155, 193-209, 1988.
Milanese, F., Rapalini, A., Slotznick, S. P., Tobin, T. S., Kirschvink, J., and Olivero, E.: Late Cretaceous paleogeography of the Antarctic Peninsula: New paleomagnetic pole from the James Ross Basin, Journal of South American Earth Sciences, 91, 131-143, 2019.
Miller, K. G., Barrera, E., Olsson, R. K., Sugarman, P. J., and Savin, S. M.: Does ice drive early Maastrichtian eustasy?, Geology, 27, 783-786, 1999.
Moiroud, M., Pucéat, E., Donnadieu, Y., Bayon, G., Guiraud, M., Voigt, S., Deconinck, J.-F., and Monna, F.: Evolution of neodymium isotopic signature of seawater during the Late Cretaceous: Implications for intermediate and deep circulation, Gondwana Research, 36, 503-522, 2016.
Monteiro, F. M., Pancost, R. D., Ridgwell, A., and Donnadieu, Y.: Nutrients as the dominant control on the spread of anoxia and euxinia across the Cenomanian‐Turonian oceanic anoxic event (OAE2): Model‐data comparison, Paleoceanography, 27, 2012.
Murphy, D. P., and Thomas, D. J.: Cretaceous deep-water formation in the Indian sector of the Southern Ocean, Paleoceanography, 27, PA1211, 10.1029/2011pa002198, 2012.
Murphy, D. P., and Thomas, D. J.: The evolution of Late Cretaceous deep‐ocean circulation in the Atlantic basins: Neodymium isotope evidence from South Atlantic drill sites for tectonic controls, Geochemistry, Geophysics, Geosystems, 14, 5323-5340, 2013.
Niezgodzki, I., Knorr, G., Lohmann, G., Tyszka, J., and Markwick, P. J.: Late Cretaceous climate simulations with different CO2 levels and subarctic gateway configurations: A model‐data comparison, Paleoceanography, 32, 980-998, 2017.
Niezgodzki, I., Tyszka, J., Knorr, G., and Lohmann, G.: Was the Arctic Ocean ice free during the latest Cretaceous? The role of CO2 and gateway configurations, Global and Planetary Change, 177, 201-212, 2019.
Nouri, F., Azizi, H., Golonka, J., Asahara, Y., Orihashi, Y., Yamamoto, K., Tsuboi, M., and Anma, R.: Age and petrogenesis of Na-rich felsic rocks in western Iran: Evidence for closure of the southern branch of the Neo-Tethys in the Late Cretaceous, Tectonophysics, 671, 151-172, 2016.

https://doi.org/10.5194/cp-2019-157
Preprint. Discussion started: 16 January 2020

Climate of the Past
Discussions

O'Brien, C. L., Robinson, S. A., Pancost, R. D., Sinninghe Damsté, J. S., Schouten, S., Lunt, D. J., Alsenz, H., Bornemann, A., Bottini, C., Brassell, S. C., Farnsworth, A., Forster, A., Huber, B. T., Inglis, G. N., Jenkyns, H. C., Linnert, C., Littler, K., Markwick, P., McAnena, A., Mutterlose, J., Naafs, B. D. A., Püttmann, W., Sluijs, A., van Helmond, N. A. G. M., Vellekoop, J., Wagner, T., and Wrobel, N. E.: Cretaceous sea-surface temperature evolution: Constraints from TEX 86 and planktonic foraminiferal oxygen isotopes, Earth-Science Reviews, 172, 224-247, 10.1016/j.earscirev.2017.07.012, 2017.

O'Connor, J. M., and Duncan, R. A.: Evolution of the Walvis Ridge ‐ Rio Grande Rise hot spot system: Implications for African and South American plate motions over plumes, Journal of Geophysical Research: Solid Earth, 95, 17475-17502, 1990.

Ortiz-Jaureguizar, E., and Pascual, R.: The tectonic setting of the Caribbean region and the K/T turnover of the South American land-mammal fauna, Boletín Geológico y Minero, 122, 333-344, 2011.

Otto-Bliesner, B. L., Brady, E. C., and Shields, C.: Late Cretaceous ocean: Coupled simulations with the National Center for Atmospheric Research Climate System Model, Journal of Geophysical Research, 107, 10.1029/2001jd000821, 2002.

Pearson, P. N.: Oxygen isotopes in foraminifera: Overview and historical review, The Paleontological Society Papers, 18, 1-38, 2012.

Piepgras, D. J., and Wasserburg, G. J.: Isotopic composition of neodymium in waters from the Drake Passage, Science, 217, 207-214, 1982.

Pindell, J. L., and Kennan, L.: Tectonic evolution of the Gulf of Mexico, Caribbean and northern South America in the mantle reference frame: an update, Geological Society, London, Special Publications, 328, 1-55, 2009.

Pletsch, T., Erbacher, J., Holbourn, A. E. L., Kuhnt, W., Moullade, M., Oboh-Ikuenobede, F. E., Söding, E., and Wagner, T.: Cretaceous separation of Africa and South America: the view from the West African margin (ODP Leg 159), Journal of South American Earth Sciences, 14, 147-174, 2001.

Poblete, F., Roperch, P., Arriagada, C., Ruffet, G., de Arellano, C. R., Hervé, F., and Poujol, M.: Late Cretaceous–early Eocene counterclockwise rotation of the Fueguian Andes and evolution of the Patagonia–Antarctic Peninsula system, Tectonophysics, 668, 15-34, 2016.

Poulsen, C. J., Seidov, D., Barron, E. J., and Peterson, W. H.: The impact of paleogeographic evolution on the surface oceanic circulation and the marine environment within the Mid ‐ Cretaceous tethys, Paleoceanography, 13, 546-559, 1998.

Poulsen, C. J., Barron, E. J., Arthur, M. A., and Peterson, W. H.: Response of the Mid-Cretaceous global oceanic circulation to tectonic and CO2 forcings, Paleoceanography, 16, 576-592, 10.1029/2000pa000579, 2001.

Poulsen, C. J., Gendaszek, A. S., and Jacob, R. L.: Did the rifting of the Atlantic Ocean cause the Cretaceous thermal maximum?, Geology, 31, 115-118, 10.1130/0091-7613(2003)031, 2003.

Price, G. D.: The evidence and implications of polar ice during the Mesozoic, Earth-Science Reviews, 48, 183-210, 1999.

Pucéat, E., Lécuyer, C., Sheppard, S. M. F., Dromart, G., Reboulet, S., and Grandjean, P.: Thermal evolution of Cretaceous Tethyan marine waters inferred from oxygen isotope composition of fish tooth enamels, Paleoceanography, 18, 1029, 10.1029/2002pa000823, 2003.

Pucéat, E., Lécuyer, C., and Reisberg, L.: Neodymium isotope evolution of NW Tethyan upper ocean waters throughout the Cretaceous, Earth and Planetary Science Letters, 236, 705-720, 2005.

Reguero, M. A., Gelfo, J. N., López, G. M., Bond, M., Abello, A., Santillana, S. N., and Marenssi, S. A.: Final Gondwana breakup: the Paleogene South American native ungulates

https://doi.org/10.5194/cp-2019-157
Preprint. Discussion started: 16 January 2020

Climate of the Past
Discussions
Open Access
EGU

and the demise of the South America–Antarctica land connection, Global and Planetary change, 123, 400-413, 2014.

Rempfer, J., Stocker, T. F., Joos, F., Dutay, J.-C., and Siddall, M.: Modelling Nd-isotopes with a coarse resolution ocean circulation model: Sensitivities to model parameters and source/sink distributions, Geochimica et Cosmochimica Acta, 75, 5927-5950, 2011.

Robinson, S. A., Murphy, D. P., Vance, D., and Thomas, D. J.: Formation of "Southern Component Water" in the Late Cretaceous: Evidence from Nd-isotopes, Geology, 38, 871-874, 10.1130/g31165.1, 2010.

Robinson, S. A., and Vance, D.: Widespread and synchronous change in deep-ocean circulation in the North and South Atlantic during the Late Cretaceous, Paleoceanography, 27, n/a-n/a, 10.1029/2011pa002240, 2012.

Roest, W. R., and Srivastava, S. P.: Sea-floor spreading in the Labrador Sea: A new reconstruction, Geology, 17, 1000-1003, 1989.

Roy, M., van de Flierdt, T., Hemming, S. R., and Goldstein, S. L.: 40Ar/39Ar ages of hornblende grains and bulk Sm/Nd isotopes of circum-Antarctic glacio-marine sediments: implications for sediment provenance in the southern ocean, Chemical Geology, 244, 507-519, 2007.

Scher, H., and Martin, E.: Timing and climatic consequences of the opening of Drake Passage, Science, 312, 428-430, 10.1126/science.1120044, 2006.

Schlanger, S. O., and Jenkyns, H. C.: Cretaceous oceanic anoxic events: causes and consequences, Geologie en mijnbouw, 55, 1976.

Sepulchre, P., Arsouze, T., Donnadieu, Y., Dutay, J. C., Jaramillo, C., Le Bras, J., Martin, E., Montes, C., and Waite, A. J.: Consequences of shoaling of the Central American Seaway determined from modeling Nd isotopes, Paleoceanography, 29, 176-189, 10.1002/2013pa002501, 2014.

Setoyama, E., Kaminski, M. A., and Tyszka, J.: Late Cretaceous–Paleogene foraminiferal morphogroups as palaeoenvironmental tracers of the rifted Labrador margin, northern proto-Atlantic, Grzybowski Foundation Special Publication, 22, 179-220, 2017.

Sewall, J. O., Van De Wal, R. S. W., Van Der Zwan, K., Van Oosterhout, C., Dijkstra, H. A., and Scotese, C. R.: Climate model boundary conditions for four Cretaceous time slices, Climate of the Past, 3, 647-657, 2007.

Shackleton, N., and Kennett, J.: Paleotemperature history of the Cenozoic and the initiation of Antarctic glaciation: oxygen and carbon isotope analyses in DSDP Sites 277, 279, and 281, Initial reports of the deep sea drilling project, 29, 743-755, 1975.

Sijp, W. P., and England, M. H.: Effect of the Drake Passage throughflow on global climate, Journal of physical oceanography, 34, 1254-1266, 10.1175/1520-0485(2004)034, 2004.

Soudry, D., Glenn, C. R., Nathan, Y., Segal, I., and VonderHaar, D.: Evolution of Tethyan phosphogenesis along the northern edges of the Arabian–African shield during the Cretaceous–Eocene as deduced from temporal variations of Ca and Nd isotopes and rates of P accumulation, Earth-Science Reviews, 78, 27-57, 2006.

Stampfli, G. M.: Tethyan oceans, Geological society, london, special publications, 173, 1-23, 2000.

Stampfli, G. M., and Borel, G. D.: A plate tectonic model for the Paleozoic and Mesozoic constrained by dynamic plate boundaries and restored synthetic oceanic isochrons, Earth and Planetary Science Letters, 196, 17-33, 2002.

Stärz, M., Jokat, W., Knorr, G., and Lohmann, G.: Threshold in North Atlantic-Arctic Ocean circulation controlled by the subsidence of the Greenland-Scotland Ridge, Nature communications, 8, 15681, 2017.

Tabor, C. R., Poulsen, C. J., Lunt, D. J., Rosenbloom, N. A., Otto-Bliesner, B. L., Markwick, P. J., Brady, E. C., Farnsworth, A., and Feng, R.: The cause of Late Cretaceous cooling: A multimodel-proxy comparison, Geology, 44, 963-966, 10.1130/g38363.1, 2016.
Tabor, C. R., Feng, R., and Otto‐Bliesner, B. L.: Climate responses to the splitting of a supercontinent: Implications for the breakup of Pangea, Geophysical Research Letters, 2019.
Tachikawa, K., Jeandel, C., and Roy-Barman, M.: A new approach to the Nd residence time in the ocean: the role of atmospheric inputs, Earth and Planetary Science Letters, 170, 433-446, 1999.
Tachikawa, K., Athias, V., and Jeandel, C.: Neodymium budget in the modern ocean and paleo-oceanographic implications, Journal of Geophysical Research, 108, 10.1029/1999jc000285, 2003.
Tachikawa, K., Arsouze, T., Bayon, G., Bory, A., Colin, C., Dutay, J.-C., Frank, N., Giraud, X., Gourlan, A. T., and Jeandel, C.: The large-scale evolution of neodymium isotopic composition in the global modern and Holocene ocean revealed from seawater and archive data, Chemical Geology, 457, 131-148, 2017.
Tarduno, J. A., Brinkman, D. B., Renne, P. R., Cottrell, R. D., Scher, H., and Castillo, P.: Evidence for extreme climatic warmth from Late Cretaceous Arctic vertebrates, Science, 282, 2241-2243, 1998.
Thomas, D. J., Korty, R., Huber, M., Schubert, J. A., and Haines, B.: Nd isotopic structure of the Pacific Ocean 70–30 Ma and numerical evidence for vigorous ocean circulation and ocean heat transport in a greenhouse world, Paleoceanography, 29, 454-469, 2014.
Toggweiler, J., and Samuels, B.: Effect of Drake Passage on the global thermohaline circulation, Deep Sea Research Part I: Oceanographic Research Papers, 42, 477-500, 1995.
Upchurch, G. R., Kiehl, J., Shields, C., Scherer, J., and Scotese, C.: Latitudinal temperature gradients and high-latitude temperatures during the latest Cretaceous: Congruence of geologic data and climate models, Geology, 43, 683-686, 10.1130/g36802.1, 2015.
Vahlenkamp, M., Niezgodzki, I., De Vleeschouwer, D., Lohmann, G., Bickert, T., and Pälike, H.: Ocean and climate response to North Atlantic seaway changes at the onset of long-term Eocene cooling, Earth and Planetary Science Letters, 498, 185-195, 2018.
van de Flierdt, T., Griffiths, A. M., Lambelet, M., Little, S. H., Stichel, T., and Wilson, D. J.: Neodymium in the oceans: a global database, a regional comparison and implications for palaeoceanographic research, Philosophical Transactions of the Royal Society A: Mathematical, Physical and Engineering Sciences, 374, 20150293, 2016.
Voigt, S., Jung, C., Friedrich, O., Frank, M., Teschner, C., and Hoffmann, J.: Tectonically restricted deep-ocean circulation at the end of the Cretaceous greenhouse, Earth and Planetary Science Letters, 369, 169-177, 2013.
Wang, Y., Huang, C., Sun, B., Quan, C., Wu, J., and Lin, Z.: Paleo-CO2 variation trends and the Cretaceous greenhouse climate, Earth-Science Reviews, 129, 136-147, 10.1016/j.earscirev.2013.11.001, 2014.
Wilson, P. A., and Norris, R. D.: Warm tropical ocean surface and global anoxia during the mid-Cretaceous period, Nature, 412, 425-429, 2001.
Ye, J., Chardon, D., Rouby, D., Guillocheau, F., Dall'asta, M., Ferry, J.-N., and Broucke, O.: Paleogeographic and structural evolution of northwestern Africa and its Atlantic margins since the early Mesozoic, Geosphere, 13, 1254-1284, 2017.
Zhou, J., Poulsen, C. J., Pollard, D., and White, T. S.: Simulation of modern and middle Cretaceous marine δ18O with an ocean‐atmosphere general circulation model, Paleoceanography, 23, 2008.

https://doi.org/10.5194/cp-2019-157
Preprint. Discussion started: 16 January 2020

Climate of the Past
Discussions

Tables and figures

Table 1 and Figures 1-15

https://doi.org/10.5194/cp-2019-157
Preprint. Discussion started: 16 January 2020

Climate of the Past Discussions

Section	Simulation	Water transport (Sv): Surface (0 - 500 m)	Intermediate (500 - 1500 m)	Deep (> 1500 m)	Total
Caribbean (>0 eastward)	Cenomanian	-20.8 (12.9 - 33.7)	-8.8 (0.9 - 9.8)	0	-29.6 (13.8 - 43.5)
	Maastrichtian	-5.5 (3.1 - 8.6)	0	0	-5.5 (3.1 - 8.6)
	Deep Labrador Seaway	-5.0 (3.3 - 8.3)	0	0	-5.0 (3.3 - 8.3)
	Deep Caribbean Seaway	-7.4 (9.7 - 17.1)	0 (0.6 - 0.6)	4.4 (4.6 - 0.2)	-3.0 (14.9 - 17.9)
	Deep Drake Passage	-5.6 (3.1 - 8.7)	0	0	-5.6 (3.1 - 8.7)
	Deep Tethys Gateway	-5.7 (3.0 - 8.7)	0	0	-5.7 (3.0 - 8.7)
Central Atlantic (>0 northward)	Cenomanian	2.7 (4.8 - 2.1)	-0.6 (0.2 - 0.8)	-0.3 (0 - 0.3)	1.8 (5.0 - 3.2)
	Maastrichtian	0.1 (7.6 - 7.5)	-1.3 (0.4 -1.6)	1.8 (2.4 - 0.6)	0.6 (10.4 - 9.7)
	Deep Labrador Seaway	0.1 (7.8 - 7.7)	-2.3 (0.6 - 2.9)	2.3 (2.8 - 0.5)	0.1 (11.2 - 11.1)
	Deep Caribbean Seaway	1.1 (8.1 - 7.0)	-0.3 (0.5 - 0.8)	-3.1 (0.5 - 3.6)	-2.3 (9.1 - 11.4)
	Deep Drake Passage	0.2 (7.4 - 7.2)	-0.7 (0.2 - 1.0)	1.3 (1.8 - 0.5)	0.8 (9.4 - 8.7)
	Deep Tethys Gateway	-0.7 (7.9 - 8.5)	-2.0 (0.5 - 2.5)	-3.0 (0.6 - 3.6)	-5.7 (9.0 - 14.6)
Drake (>0 Pacific to Atlantic)	Cenomanian	0.4 (0.7 - 0.4)	0.4 (0.4 - 0)	0	0.7 (1.1 - 0.4)
	Maastrichtian	1.4 (3.2 - 1.8)	0	0	1.4 (3.2 - 1.8)
	Deep Labrador Seaway	1.2 (2.9 - 1.8)	0	0	1.2 (2.9 - 1.8)
	Deep Caribbean Seaway	1.3 (3.2 - 1.9)	0	0	1.3 (3.2 - 1.9)
	Deep Drake Passage	1.6 (4.1 - 2.4)	2.1 (2.4 - 0.3)	3.6 (4.5 - 0.9)	7.3 (11.0 - 3.6)
	Deep Tethys Gateway	1.2 (2.9 - 1.7)	0	0	1.2 (2.9 - 1.7)
East Indian (>0 northward)	Cenomanian	14.4 (14.5 - 0.1)	3.5 (4.2 - 0.7)	-1.5 (0.4 - 1.9)	16.4 (19.1 - 2.7)
	Maastrichtian	5.6 (23.2 - 17.6)	4.4 (9.1 - 4.7)	-3.7 (8.6 - 12.4)	6.3 (40.9 - 34.7)
	Deep Labrador Seaway	5.4 (23.2 - 17.8)	4.9 (9.6 - 4.7)	-3.9 (9.1 - 13.1)	6.4 (41.9 - 35.6)
	Deep Caribbean Seaway	5.4 (23.5 - 18.1)	4.1 (9.4 - 5.4)	-2.7 (10.0 - 12.7)	6.7 (42.9 - 36.2)
	Deep Drake Passage	4.8 (22.8 - 18.0)	4.9 (8.5 - 3.6)	-1.1 (7.0 - 8.1)	8.7 (38.3 - 29.7)
	Deep Tethys Gateway	4.9 (24.0 - 19.0)	4.6 (9.7 - 5.1)	-3.3 (9.1 - 12.3)	6.3 (42.8 - 36.4)
Indo-Asian (>0 Tethys to Indo-Pac.)	Cenomanian	-7.2 (44.4 - 51.6)	-5.2 (8.3 - 13.5)	-1.6 (12.7 - 14.2)	-14.0 (65.4 - 79.3)
	Maastrichtian	-8.9 (15.1 - 23.9)	1.2 (2.9 - 1.6)	-2.6 (2.9 - 5.5)	-10.2 (20.9 - 31.0)
	Deep Labrador Seaway	-8.8 (15.8 - 24.6)	1.7 (3.2 - 1.6)	-2.8 (2.9 - 5.8)	-9.9 (21.9 - 32.0)
	Deep Caribbean Seaway	-9.8 (14.2 - 24.0)	1.7 (3.1 - 1.4)	0 (6.3 - 6.3)	-8.1 (23.6 - 31.7)
	Deep Drake Passage	-9.5 (16.1 - 25.6)	3.4 (4.2 - 0.8)	-0.7 (2.8 - 3.4)	-6.8 (23.1 - 29.8)
	Deep Tethys Gateway	-9.6 (13.9 - 23.5)	3.7 (4.2 - 0.6)	-4.3 (2.4 - 6.7)	-10.3 (20.5 - 30.8)
Indonesian (>0 eastward)	Cenomanian	6.4 (51.9 - 45.5)	0.7 (14.8 - 14.1)	-4.4 (13.2 - 17.6)	2.8 (79.9 - 77.2)
	Maastrichtian	11.4 (58.2 - 46.8)	4.7 (11.6 - 6.9)	-7.4 (8.1 - 15.5)	8.8 (77.9 - 69.2)
	Deep Labrador Seaway	10.7 (57.5 - 46.8)	5.4 (11.9 - 6.5)	-7.7 (8.3- 16.0)	8.3 (77.7 - 69.3)
	Deep Caribbean Seaway	11.1 (59.8 - 48.7)	4.9 (12.0 - 7.0)	-3.7 (11.1 - 14.8)	12.3 (82.9 - 70.5)
	Deep Drake Passage	9.7 (54.8 - 45.1)	6.4 (12.7 - 6.3)	-2.4 (7.2 - 9.7)	13.7 (74.7 - 61.1)
	Deep Tethys Gateway	10.4 (56.5 - 46.1)	6.6 (12.8 - 6.2)	-8.7 (6.6 - 15.3)	8.4 (75.9 - 67.6)
Mediterranean (>0 eastward)	Cenomanian	-22.9 (0.9 - 23.8)	-3.6 (0 - 3.7)	-1.7 (0 - 1.7)	-28.2 (0.9 - 29.2)
	Maastrichtian	-6.6 (0.5 - 7.1)	0.2 (0.4 - 0.2)	0.2 (0.2 - 0)	-6.3 (1.1 - 7.3)
	Deep Labrador Seaway	-6.9 (0.4 - 7.3)	0.2 (0.4 - 0.2)	0.1 (0.1- 0)	-6.5 (0.9 - 7.5)
	Deep Caribbean Seaway	-6.8 (0.4 - 7.2)	0.1 (0.3 - 0.2)	0.2 (0.2 - 0)	-6.5 (0.9 - 7.4)
	Deep Drake Passage	-6.5 (0.5 - 7.0)	0.2 (0.4 - 0.2)	0.1 (0.1 - 0)	-6.2 (1.0 - 7.2)
	Deep Tethys Gateway	-9.1 (1.9 - 11.0)	0.5 (3.4 - 2.9)	-4.7 (0.9 - 5.7)	-13.3 (6.2 - 19.6)
South African (>0 eastward)	Cenomanian	-1.4 (1.4 - 2.8)	1.7 (2.6 - 0.9)	-0.7 (0.1 - 0.8)	-0.4 (4.1 - 4.5)
	Maastrichtian	3.0 (13.4 - 10.3)	2.6 (8.2 - 5.7)	-4.1 (3.2 - 7.3)	1.5 (24.8 - 23.3)
	Deep Labrador Seaway	2.7 (12.7 - 10.0)	3.7 (8.5 - 5.1)	-4.3 (3.1 - 7.5)	1.7 (24.3 - 22.6)
	Deep Caribbean Seaway	1.8 (14.1 - 12.3)	1.9 (6.9 - 5.0)	0.6 (3.9 - 3.3)	4.4 (24.9 - 20.6)
	Deep Drake Passage	2.3 (12.4 - 10.1)	3.9 (8.2 - 4.4)	1.0 (3.9 - 2.9)	7.2 (24.5 - 17.4)
	Deep Tethys Gateway	3.3 (14.7 - 11.5)	4.0 (8.6 - 4.6)	0.3 (3.5 - 3.2)	7.6 (26.8 - 19.3)
South Atlantic (>0 northward)	Cenomanian	1.8 (6.4 - 4.6)	-0.8 (1.1 - 1.9)	-0.1 (0.2 - 0.3)	0.9 (7.7 - 6.8)
	Maastrichtian	0 (15.2 - 15.2)	-2.5 (3.9 - 6.4)	3.1 (4.1 - 1.0)	0.6 (23.2 - 22.6)
	Deep Labrador Seaway	0.1 (15.2 - 15.0)	-3.5 (3.6 - 7.1)	3.5 (4.7 - 1.2)	0.1 (23.5 - 23.3)
	Deep Caribbean Seaway	0.8 (15.3 - 14.5)	-1.0 (3.6 - 4.6)	-2.1 (2.0 - 4.0)	-2.3 (20.9 - 23.1)
	Deep Drake Passage	0 (14.8 - 14.8)	-1.5 (4.2 - 5.7)	2.3 (3.2 - 0.9)	0.8 (22.2 - 21.4)
	Deep Tethys Gateway	-0.6 (15.4 - 15.9)	-3.2 (3.7 - 6.9)	-1.9 (1.7 - 3.6)	-5.7 (20.8 - 26.4)
South China (>0 eastward)	Cenomanian	-24.7 (0.9 - 25.6)	-4.2 (0 - 4.3)	0	-28.9 (0.9 - 29.9)
	Maastrichtian	0	0	0	0
	Deep Labrador Seaway	0	0	0	0
	Deep Caribbean Seaway	0	0	0	0
	Deep Drake Passage	0	0	0	0
	Deep Tethys Gateway	0	0	0	0
Tethys (>0 Tethys to Indo-Pac.)	Cenomanian	-20.7 (10.2 - 30.9)	-3.1 (3.5 - 6.7)	-0.4 (3.7 - 4.1)	-24.3 (17.4 - 41.7)
	Maastrichtian	-6.3 (7.8 - 14.1)	1.5 (2.9 - 1.4)	0 (1.2 - 1.2)	-4.8 (11.9 - 16.7)
	Deep Labrador Seaway	-6.3 (8.2 - 14.5)	1.5 (3.0 - 1.4)	0 (1.2 - 1.2)	-4.8 (12.4 - 17.1)
	Deep Caribbean Seaway	-6.5 (7.5 - 14.0)	1.5 (2.7 - 1.3)	0 (1.3 - 1.3)	-5.0 (11.5 - 16.6)
	Deep Drake Passage	-6.9 (7.3 - 14.2)	2.2 (3.8 - 1.6)	0 (1.2 - 1.2)	-4.7 (12.3 - 17.0)
	Deep Tethys Gateway	-8.1 (4.4 - 12.5)	1.8 (2.8 - 1.0)	-5.4 (1.5 - 6.9)	-11.7 (8.7 - 20.4)
West Indian (>0 northward) – Ceno.	Cenomanian	-16.6 (0 - 16.6)	0	0	-16.6 (0 - 16.6)
West Indian – Maas. Western side	Maastrichtian	-6.8 (1.7 - 8.5)	0.5 (0.8 - 0.3)	-0.1 (0.1 - 0.2)	-6.4 (2.6 - 9.0)
	Deep Labrador Seaway	-7.0 (1.8 - 8.7)	1.0 (1.3 - 0.3)	-0.1 (0.1 - 0.1)	-6.1 (3.2 - 9.2)
	Deep Caribbean Seaway	-7.7 (1.7 - 9.4)	-0.7 (0.3 - 1.0)	0 (0.1 - 0.1)	-8.4 (2.1 - 10.5)
	Deep Drake Passage	-7.1 (1.7 - 8.8)	0.7 (1.0 - 0.3)	0.1 (0.1 - 0)	-6.4 (2.8 - 9.1)
	Deep Tethys Gateway	-6.1 (1.8 - 7.9)	1.1 (1.2 - 0.1)	0.1 (0.1 - 0)	-5.0 (3.1 - 8.0)
West Indian – Maas. Eastern side	Maastrichtian	3.5 (5.1 - 1.6)	-0.6 (0.6 - 1.2)	-1.2 (0.3 - 1.5)	1.6 (6.0 - 4.3)
	Deep Labrador Seaway	3.5 (5.0 - 1.5)	-0.6 (0.6 - 1.2)	-1.5 (0.2 - 1.7)	1.4 (5.8 - 4.4)
	Deep Caribbean Seaway	3.9 (5.4 - 1.5)	0.8 (1.6 - 0.8)	1.3 (1.9 - 0.6)	6.0 (8.9 - 2.9)
	Deep Drake Passage	3.7 (5.3 - 1.5)	1.0 (1.4 - 0.4)	0.1 (0.4 - 0.3)	4.9 (7.1 - 2.2)
	Deep Tethys Gateway	3.9 (5.4 - 1.6)	0.8 (1.7 - 0.9)	1.7 (2.4 - 0.7)	6.3 (9.5 - 3.2)

Simulation: Cenomanian, Maastrichtian, Deep Labrador Seaway, Deep Caribbean Seaway, Deep Drake Passage, Deep Tethys Gateway

Table 1. Water transport across major oceanic sections (shown on Fig. 5) for each simulation. For each section is shown the direction of the positive transport across the gateway. There is bidirectional

https://doi.org/10.5194/cp-2019-157
Preprint. Discussion started: 16 January 2020

Climate of the Past
Discussions
Open Access

flow, i.e. positive and negative water fluxes, across most sections. The sum of positive and negative fluxes across a section gives the net water transport across the section. The net water transport, as well as positive and negative fluxes in brackets, is shown for three depth ranges (upper, intermediate and deep ocean) and for the total vertical extension of the section. The sign of the net water transport therefore gives the direction of the larger water flux across a section. Positive and negative fluxes are represented on Figs. 5 and 6 for the intermediate and deep ocean respectively.

1452

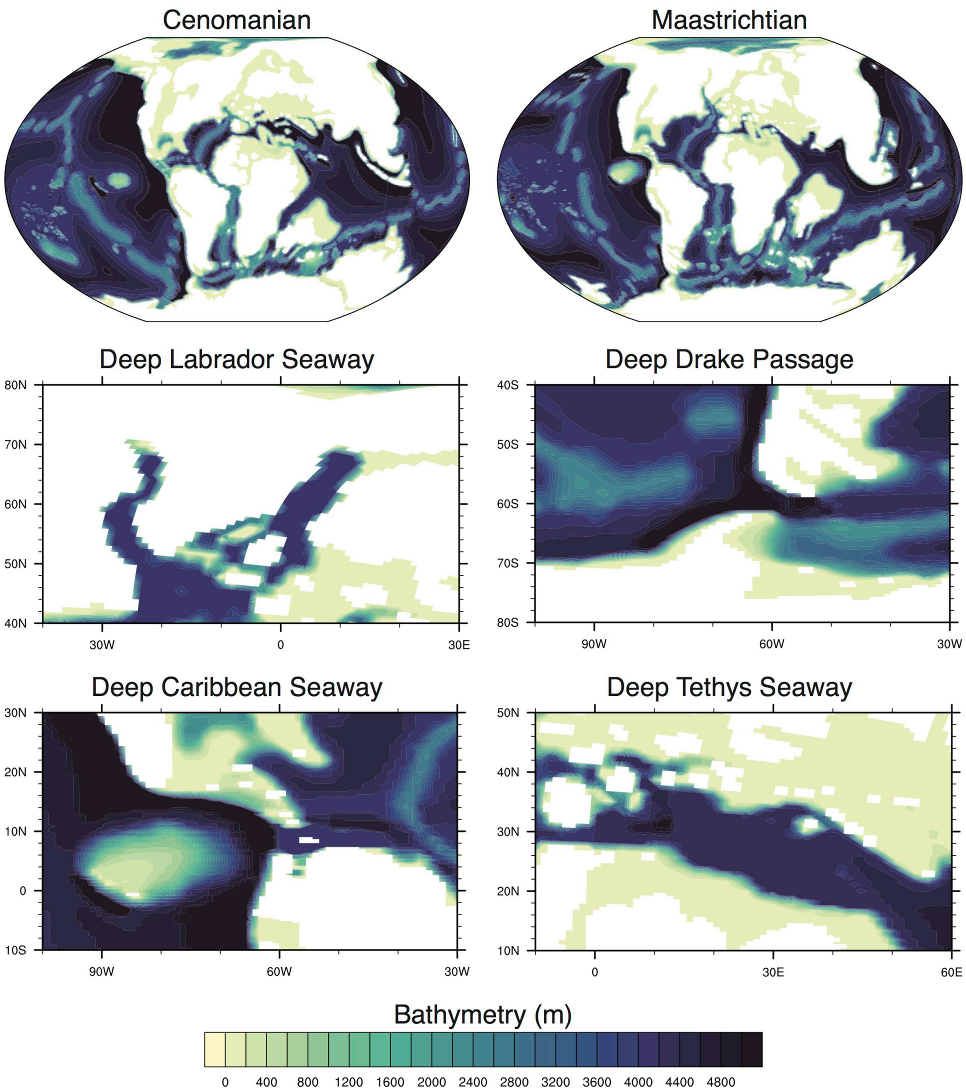

Figure 1. Bathymetry of the Cenomanian and Maastrichtian configurations and zoom on the bathymetric changes performed for each gateway sensitivity simulation.

https://doi.org/10.5194/cp-2019-157
Preprint. Discussion started: 16 January 2020

Climate of the Past
Discussions

1453

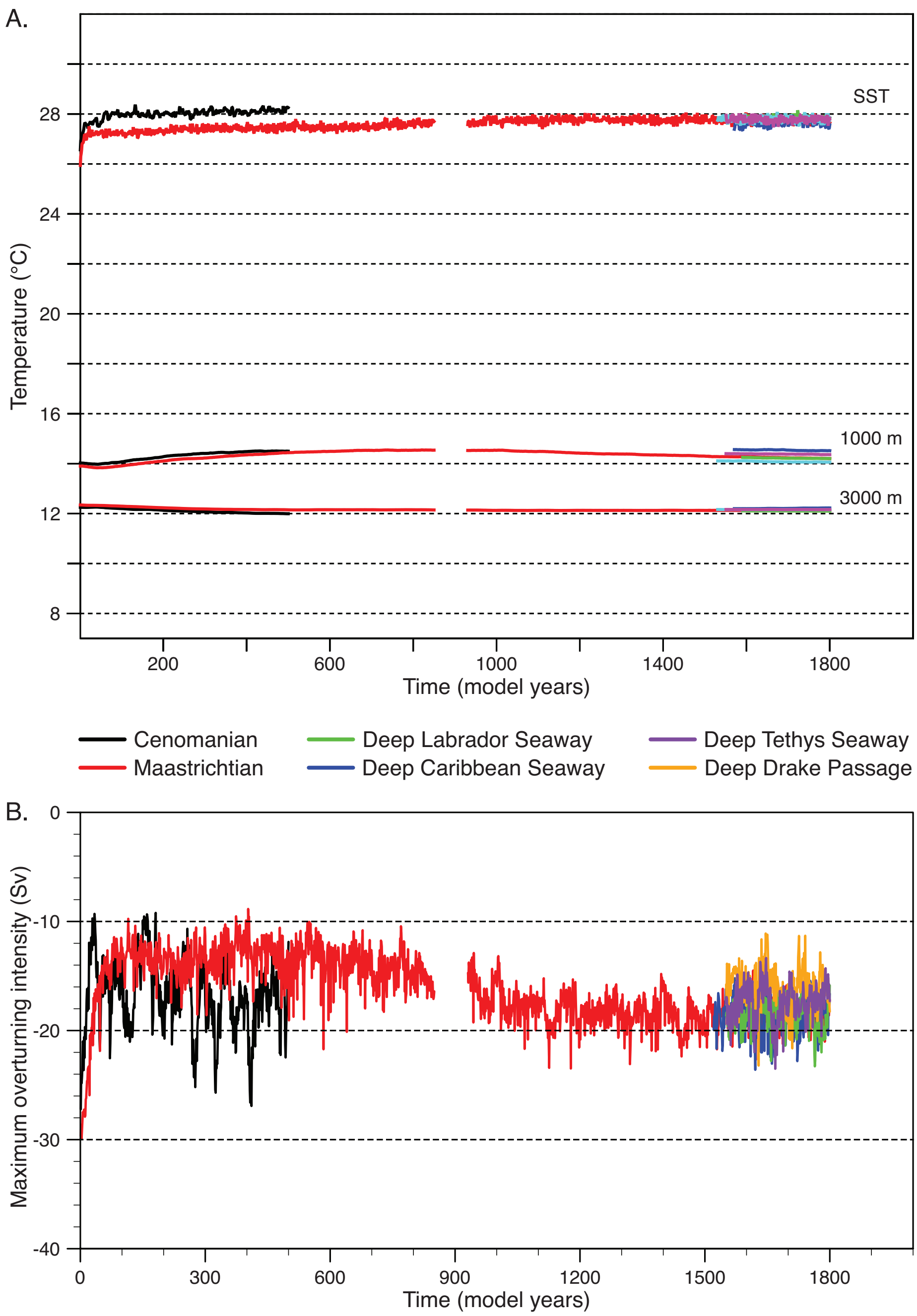

https://doi.org/10.5194/cp-2019-157
Preprint. Discussion started: 16 January 2020

Climate of the Past
Discussions

Figure 2. (A) Timeseries of temperature at the sea surface and in the intermediate (1000 m) and deep (3000 m) ocean, showing that the model has reached quasi-equilibrium at the end of the simulations. The gap between years 850 and 930 in the Maastrichtian simulation (red line) is due to unfortunate loss of data. Only the end of the sensitivity simulations is shown because the full history of the temperature evolution of these simulations was not conserved. Note that the first 1500 years of the simulations, described in Tabor et al. (2016), are omitted on this figure. (B) Timeseries of the meridional overturning circulation. Note that the maximum overturning intensity is negative because the circulation is anticlockwise.

https://doi.org/10.5194/cp-2019-157
Preprint. Discussion started: 16 January 2020

Climate of the Past Discussions

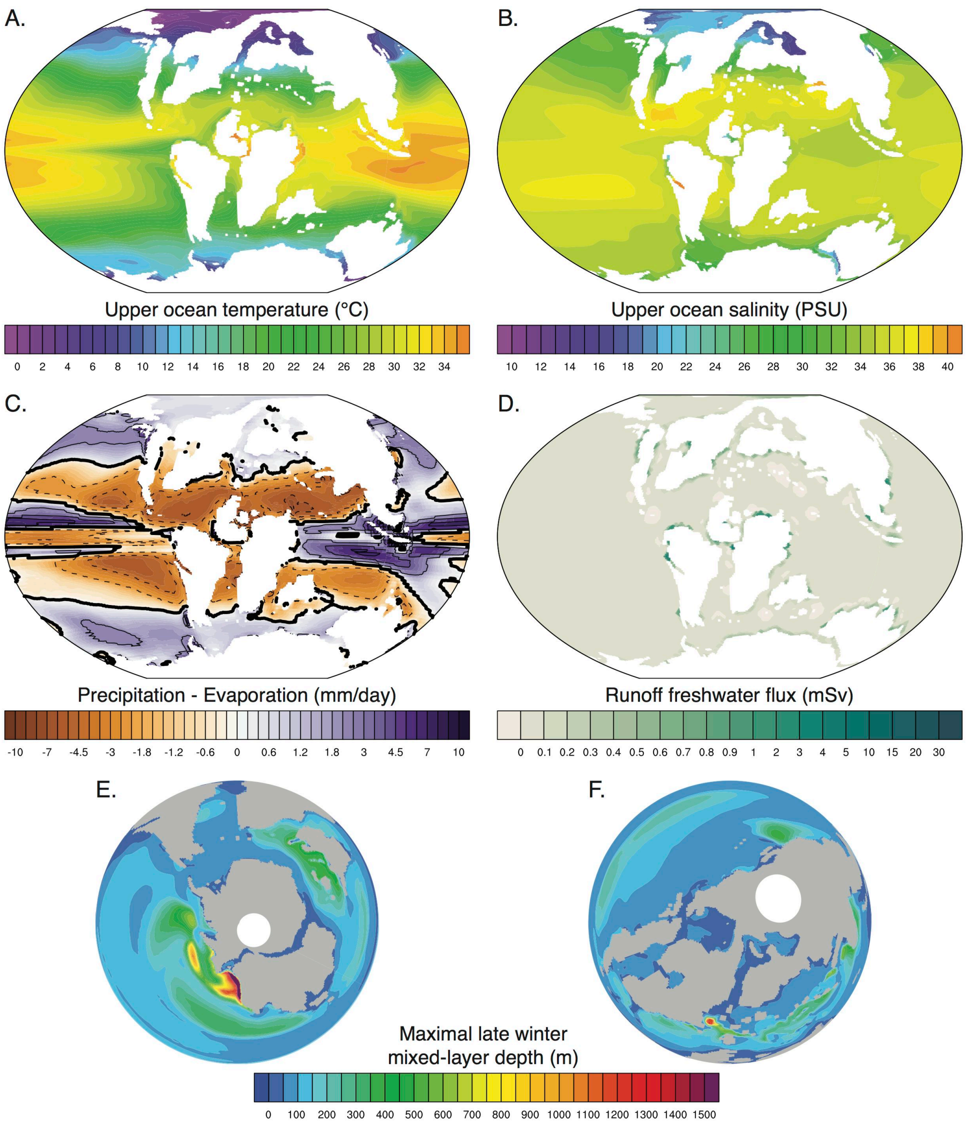

Figure 3. Climate diagnostics for the Cenomanian simulation. (A) Surface ocean (first 100 m) temperature (°C), (B) Surface ocean (first 100 m) salinity (PSU), (C) Precipitation minus evaporation (mm/day), (D) Runoff freshwater flux (mSv), (E and F) Late winter maximal mixed layer depth (m).

1455

https://doi.org/10.5194/cp-2019-157
Preprint. Discussion started: 16 January 2020

Climate of the Past Discussions
Open Access

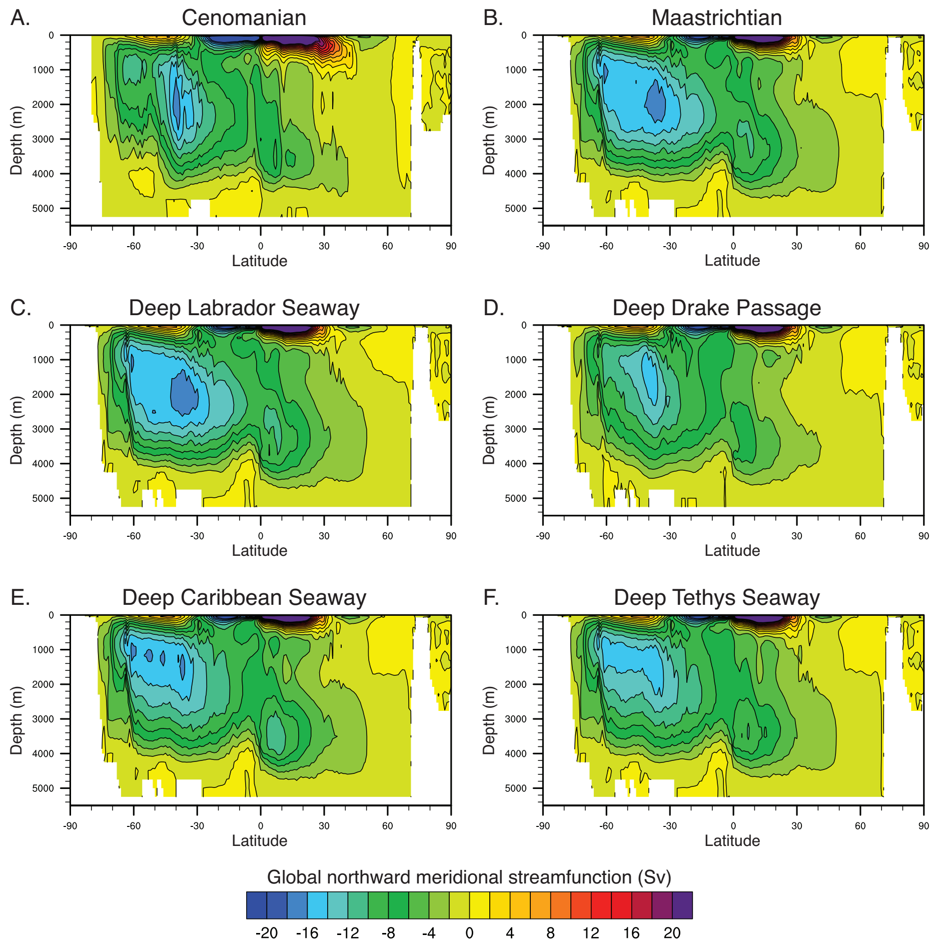

Figure 4. Global meridional overturning circulation (clockwise positive) for each experiment. (A) Cenomanian, (B) Maastrichtian, (C) Deep Labrador Seaway, (D) Deep Drake Passage, (E) Deep Caribbean Seaway, (F) Deep Tethys Seaway.

1456

https://doi.org/10.5194/cp-2019-157
Preprint. Discussion started: 16 January 2020

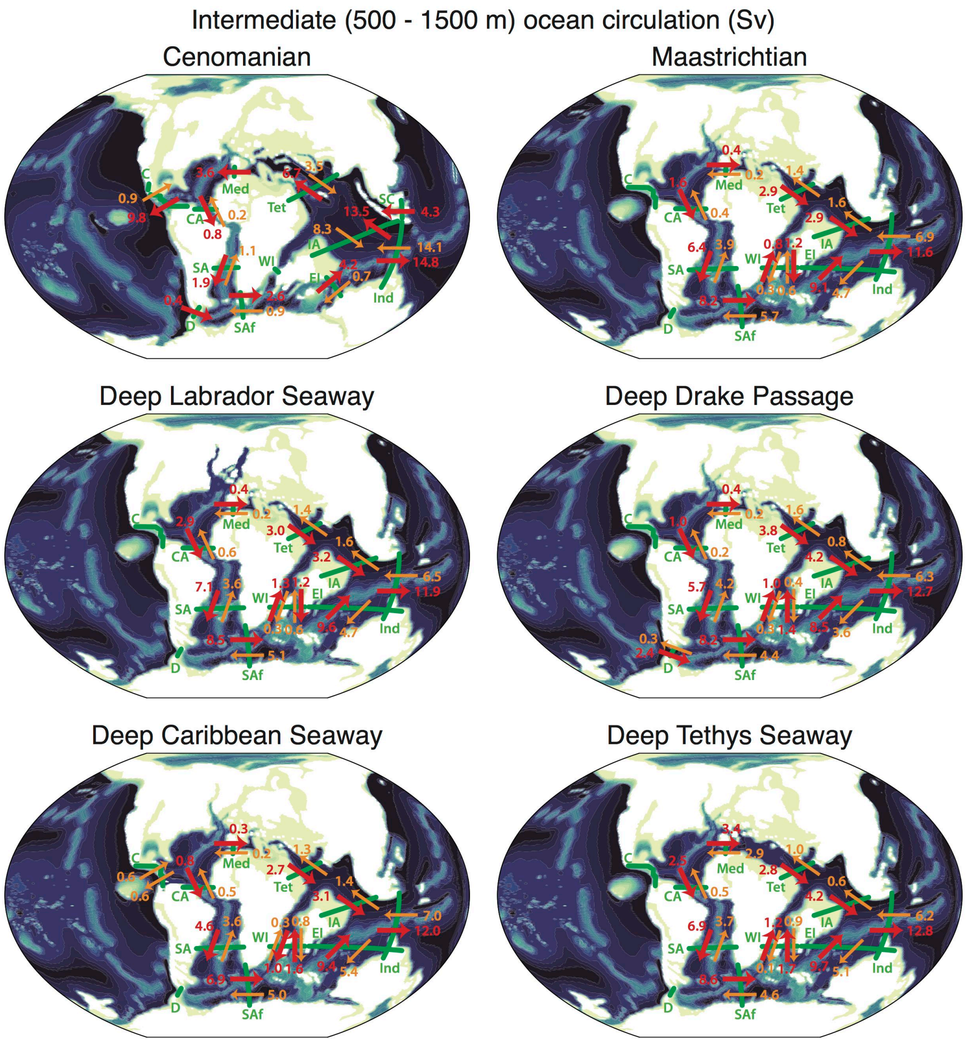

Figure 5. Intermediate (500 – 1500 m) water flow across major oceanic sections defined in Table 1 and represented in green for each simulation. The larger flux across each section is shown in red and the smaller in orange. The direction of the red arrow therefore gives the direction of the net intermediate flow across a section, the magnitude of which is given by the difference between the fluxes represented by the red and orange arrows. Abbreviated sections: C (Caribbean), CA (Central Atlantic), D (Drake), EI (East Indian), IA (Indo-Asian), Ind (Indonesian), Med (Mediterranean), SA (South Atlantic), SAf (South African), SC (South China), Tet (Tethys), WI (West Indian).

https://doi.org/10.5194/cp-2019-157
Preprint. Discussion started: 16 January 2020

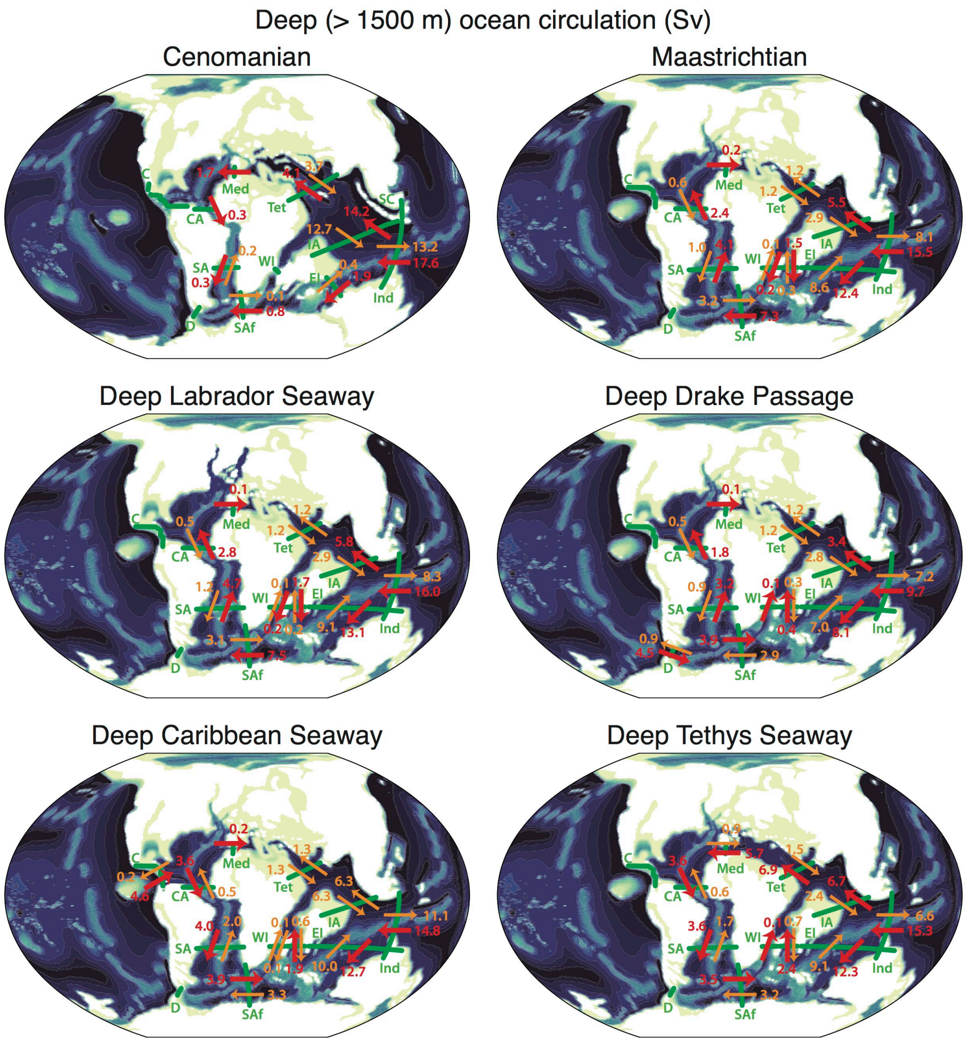

Figure 6. Deep (> 1500 m) water flow across major oceanic sections defined in Table 1 and represented in green for each simulation. Refer to the legend of Fig. 5 for additional details and abbreviations.

https://doi.org/10.5194/cp-2019-157
Preprint. Discussion started: 16 January 2020

Climate of the Past Discussions
Open Access
EGU

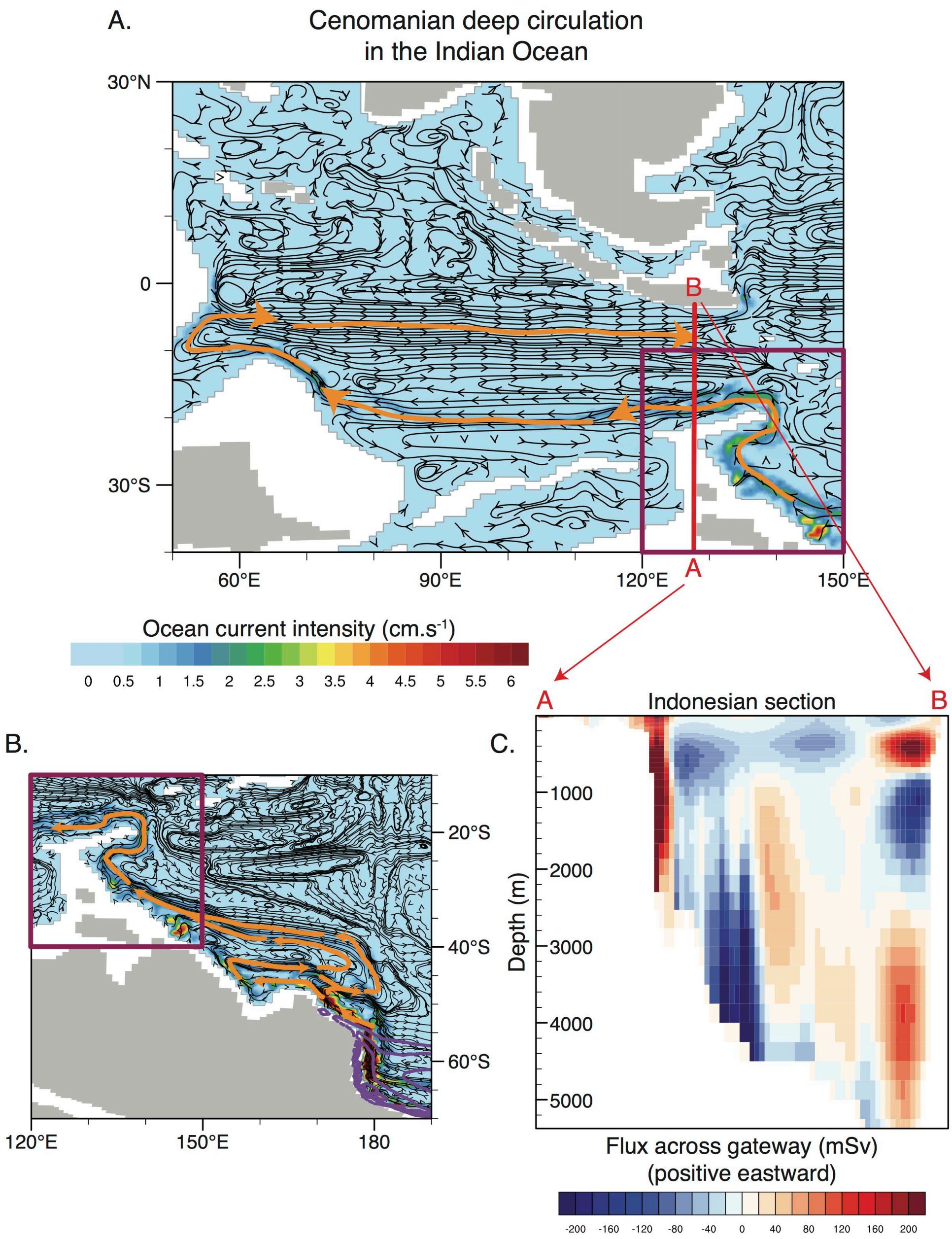

Figure 7. Cenomanian deep circulation (3000 m) in (A) the Indian Ocean and (B) the southwest Pacific Ocean. Orange arrows represent major deep current systems in the Indian Ocean and southwest Pacific. Purple contours represent regions of deep waters formation (contour 500 m). Section A-B defines the Indonesian section of Table 1. (C) Fluxes of water across the Indonesian section over the whole water column.

1459

https://doi.org/10.5194/cp-2019-157
Preprint. Discussion started: 16 January 2020

Climate of the Past
Discussions

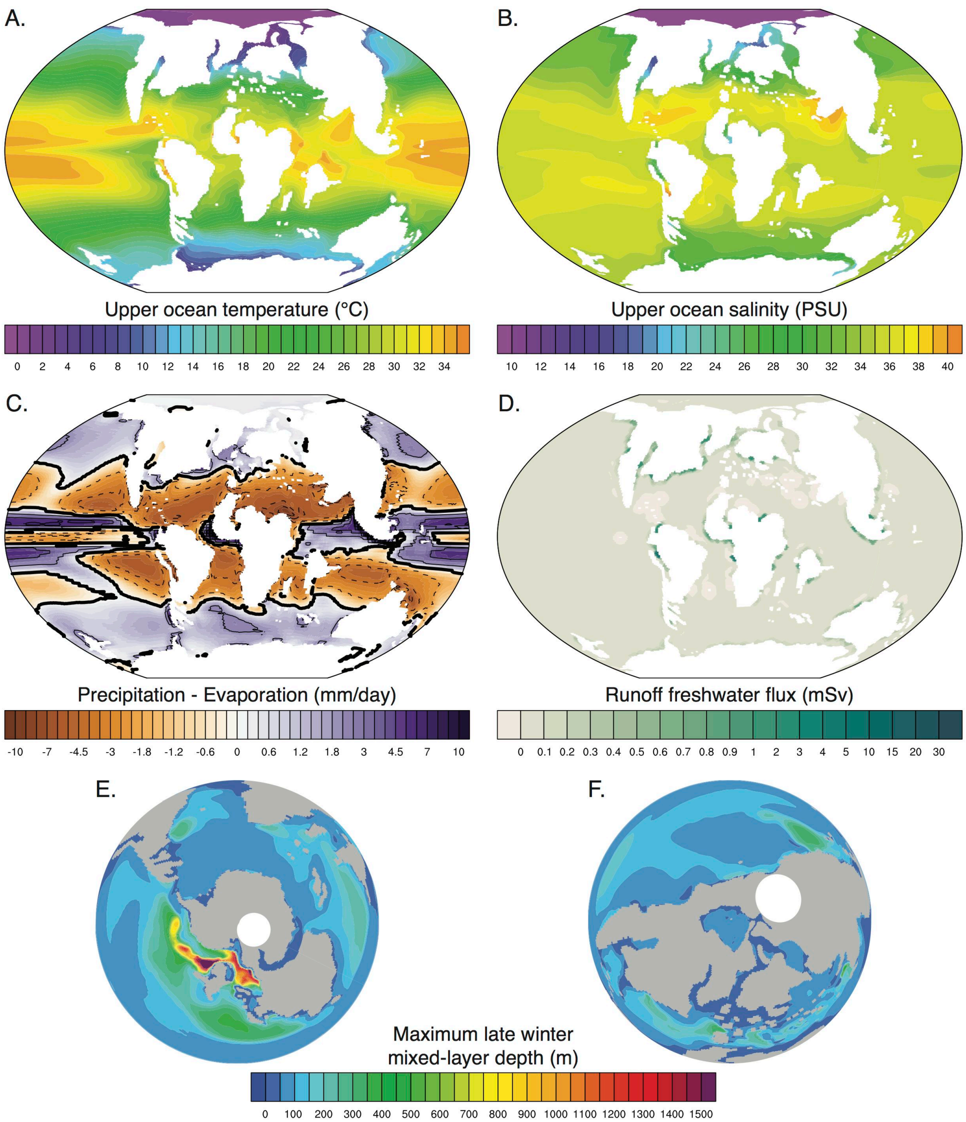

Figure 8. Climate diagnostics for the Maastrichtian simulation. (A) Surface ocean (first 100 m) temperature (°C), (B) Surface ocean (first 100 m) salinity (PSU), (C) Precipitation minus evaporation (mm/day), (D) Runoff freshwater flux (mSv), (E and F) Late winter maximal mixed layer depth (m).

https://doi.org/10.5194/cp-2019-157
Preprint. Discussion started: 16 January 2020

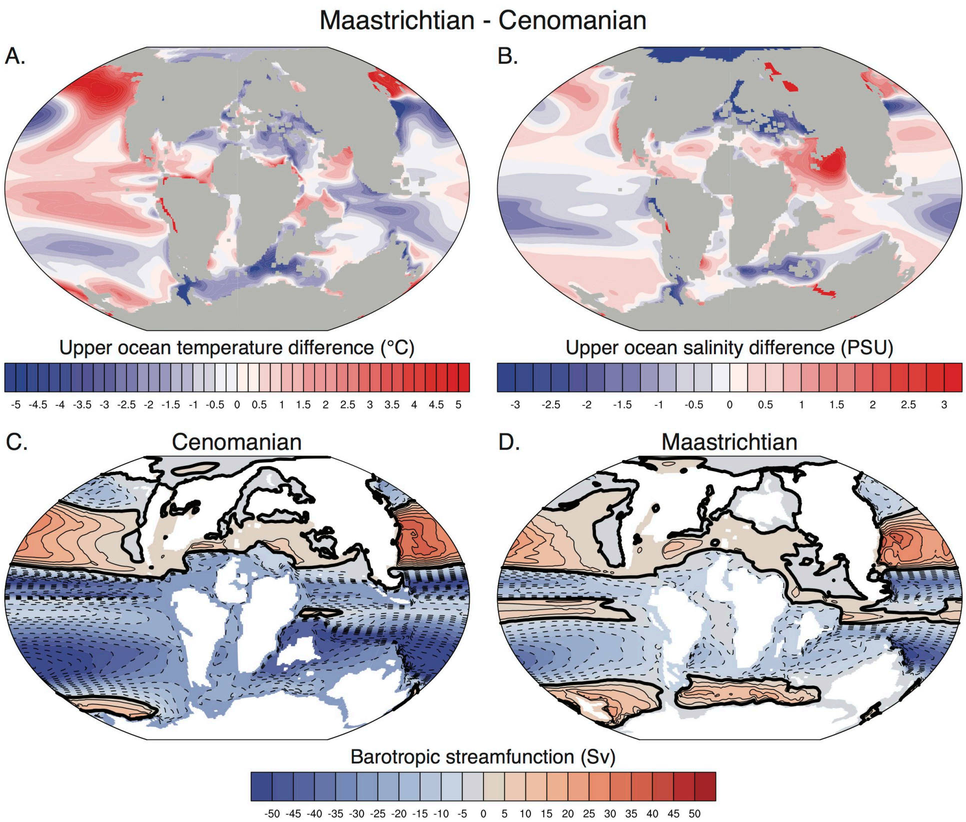

Figure 9. Climate diagnostics for the Maastrichtian simulation relative to the Cenomanian simulation. (A) Surface ocean (first 100 m) temperature difference (°C), (B) Surface ocean (first 100 m) salinity difference (°C), (C and D) Cenomanian and Maastrichtian barotropic streamfunction (Sv).

1461

https://doi.org/10.5194/cp-2019-157
Preprint. Discussion started: 16 January 2020

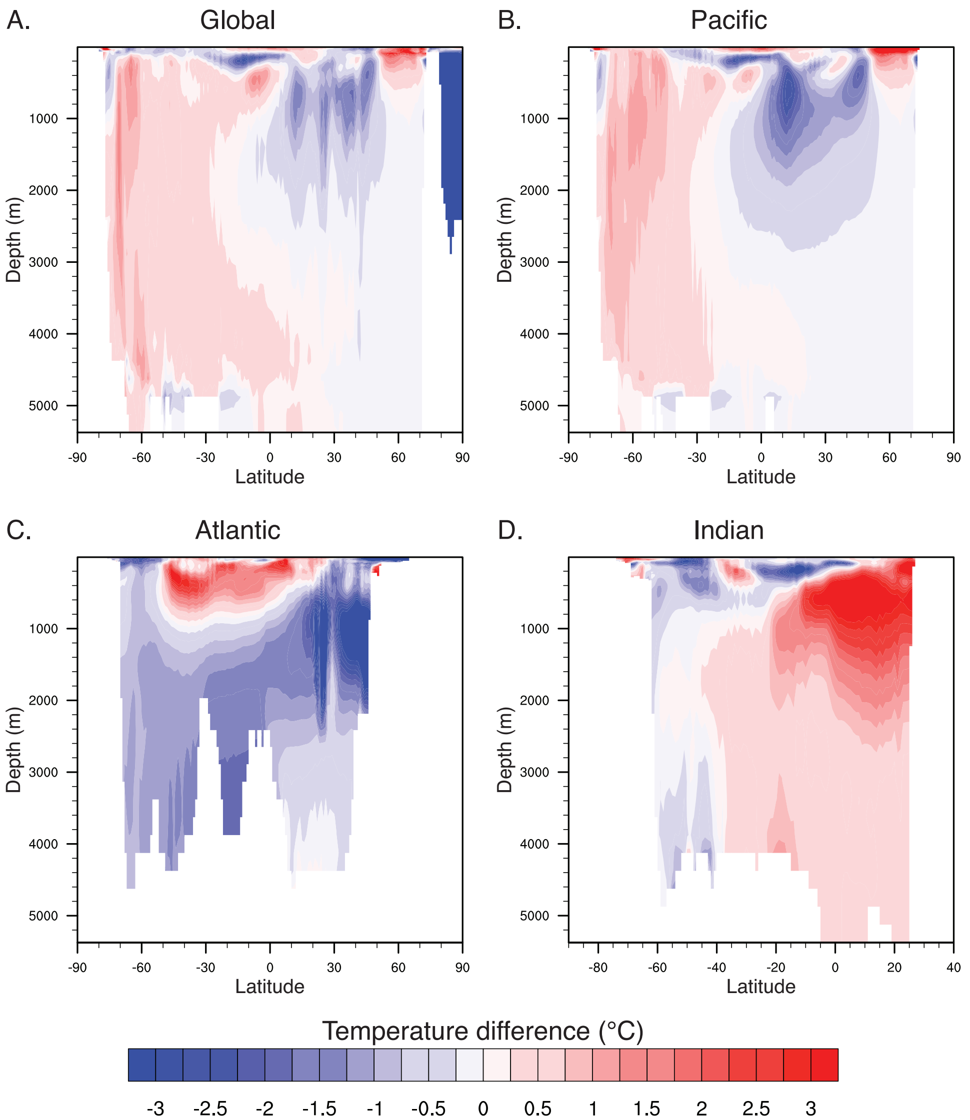

Figure 10. Zonally averaged temperature difference (°C) between the Maastrichtian and the Cenomanian simulations. (A) Global average, (B, C, D) Pacific, Atlantic and Indian average, based on basins defined in Fig. S3.

https://doi.org/10.5194/cp-2019-157
Preprint. Discussion started: 16 January 2020

Climate of the Past
Discussions
Open Access

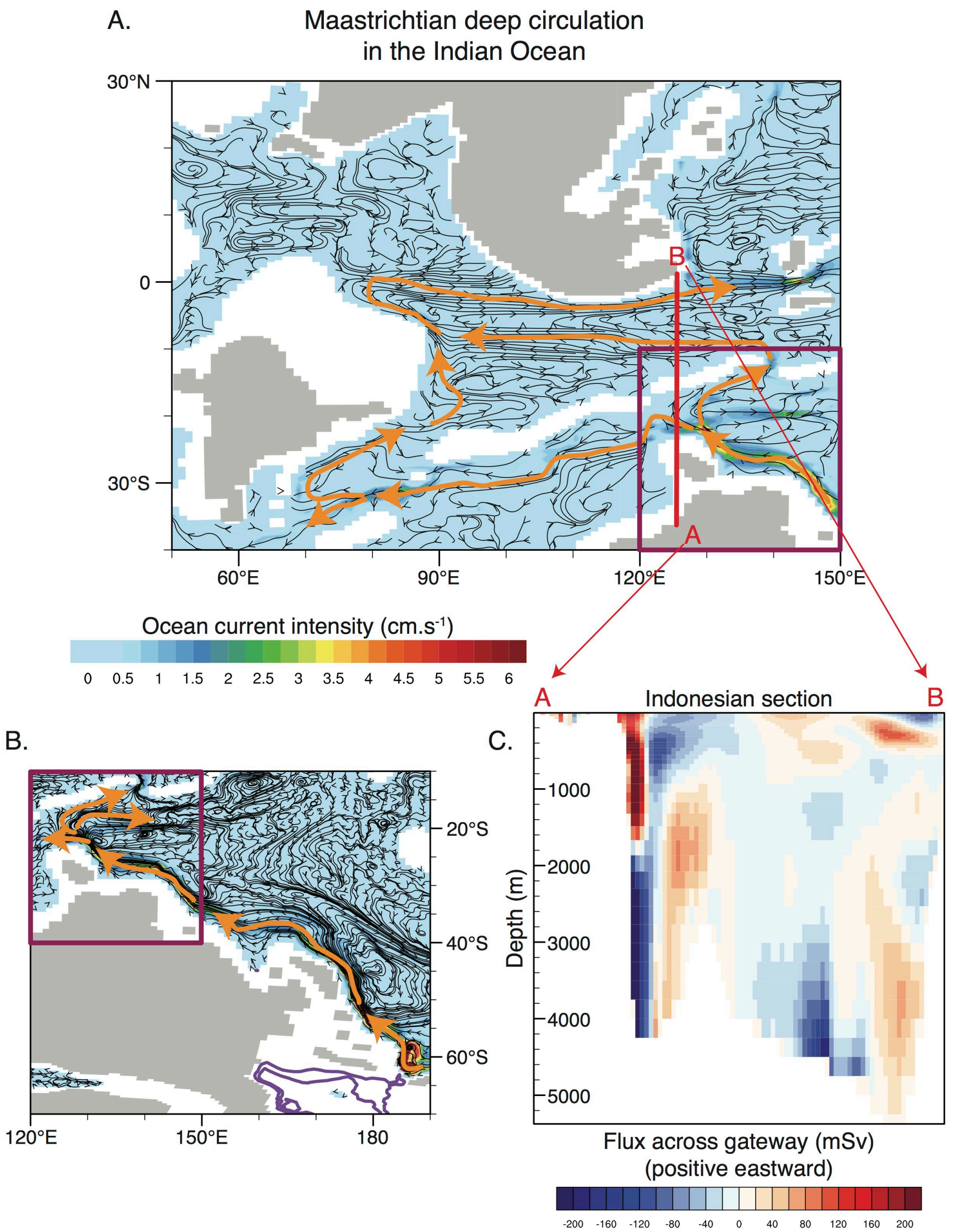

Figure 11. Maastrichtian deep circulation (3000 m) in (A) the Indian Ocean and (B) the southwest Pacific Ocean. Orange arrows represent major deep current systems in the Indian Ocean and southwest Pacific. Purple contours represent regions of deep waters formation (contour 500 m). Section A-B defines the Indonesian section of Table 1. (C) Fluxes of water across the Indonesian section over the whole water column.

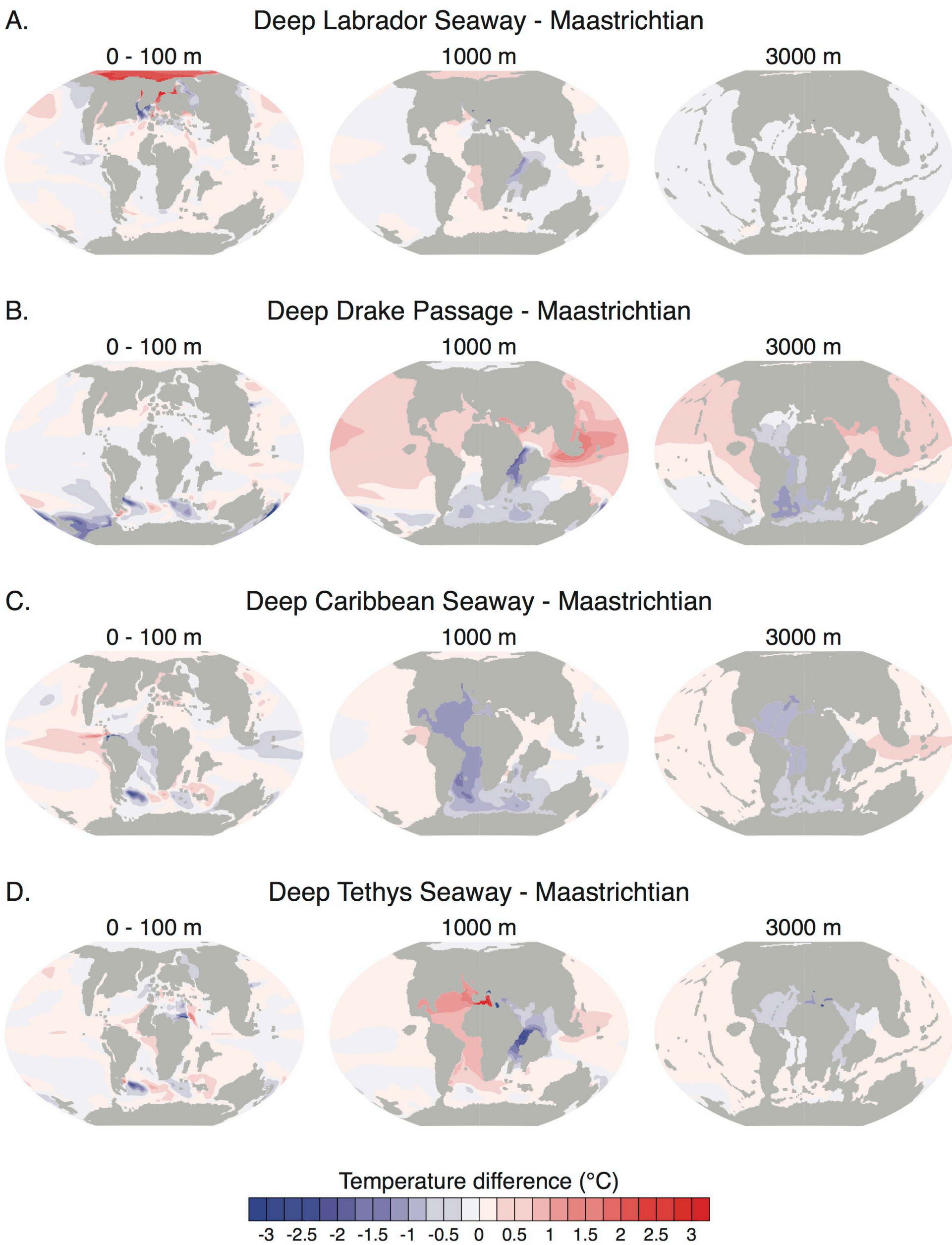

Figure 12. Surface, intermediate and deep ocean temperature difference (°C) between the gateway sensitivity experiments and the Maastrichtian simulation.

1464

https://doi.org/10.5194/cp-2019-157
Preprint. Discussion started: 16 January 2020

Climate of the Past
Discussions

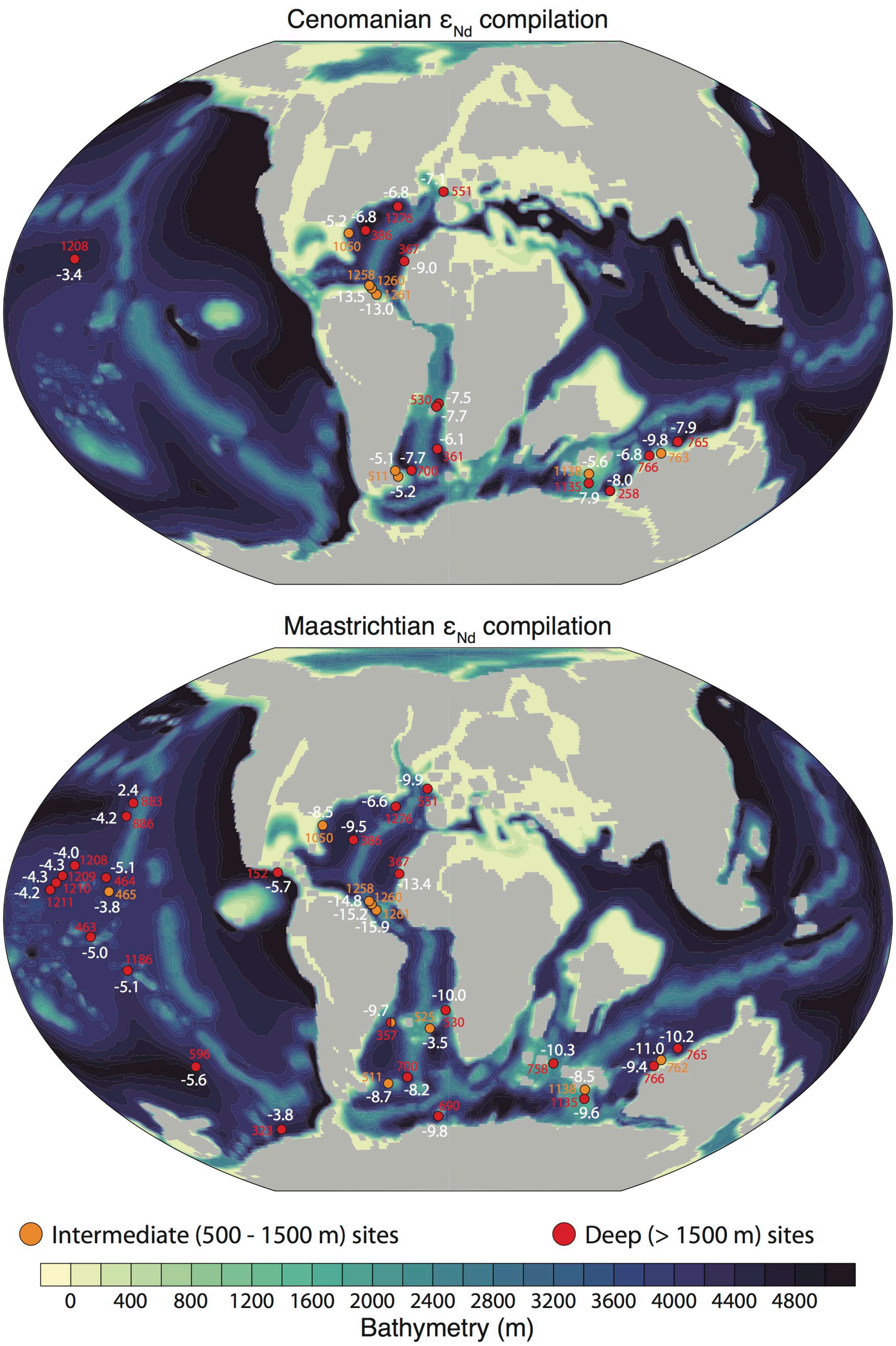

Figure 13. Cenomanian and Maastrichtian ε_{Nd} compilation based on the review of Moiroud et al. (2016), with few additions (Tables S2 and S3). ε_{Nd} values at each site are averaged between 100 Ma

https://doi.org/10.5194/cp-2019-157
Preprint. Discussion started: 16 January 2020

Climate of the Past Discussions

and 90 Ma for the Cenomanian and between 75 Ma and 65 Ma for the Maastrichtian. Site numbers are shown for clarity.

1465

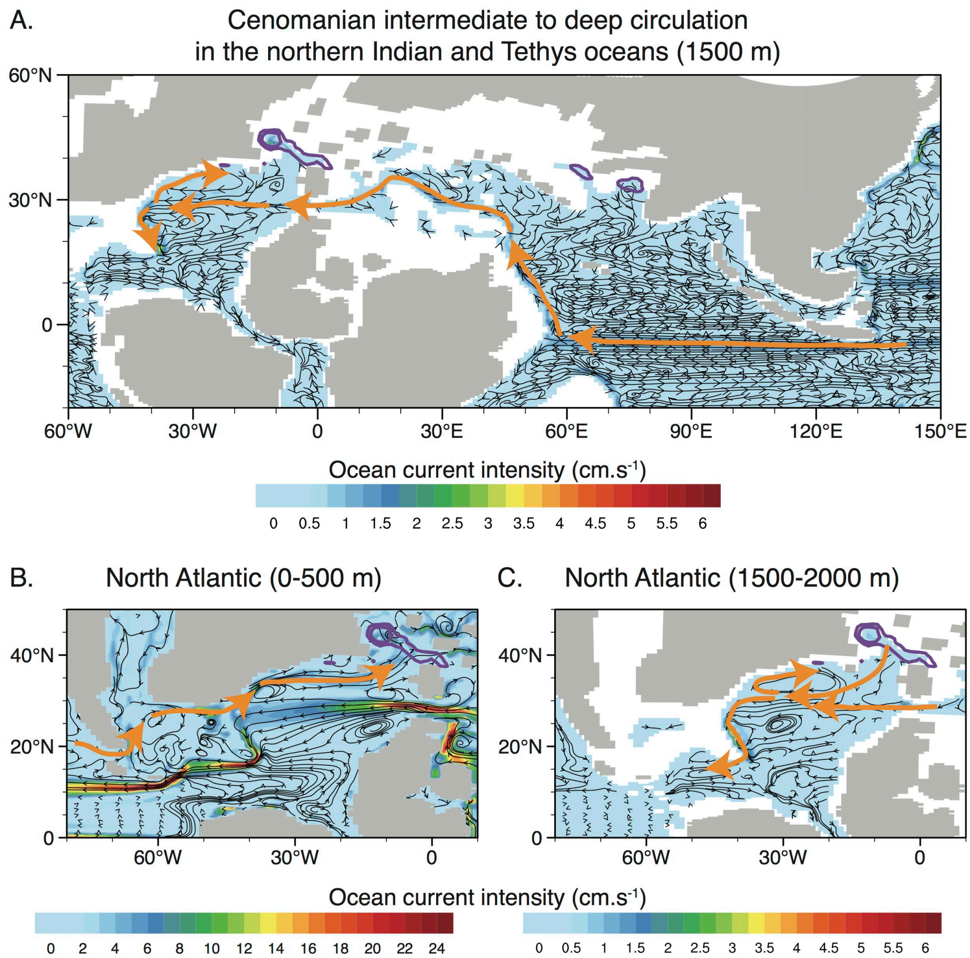

Figure 14. Cenomanian ocean circulation in (A) the northern Indian and Tethys Oceans at 1500 m depth, (B) the North Atlantic Ocean between 0 and 500 m depth and (C) the North Atlantic Ocean between 1500 and 2000 m depth. Orange contours represent major pathways of water masses. Purple contours are the maximal winter MLD (500 m contours).

1466

https://doi.org/10.5194/cp-2019-157
Preprint. Discussion started: 16 January 2020

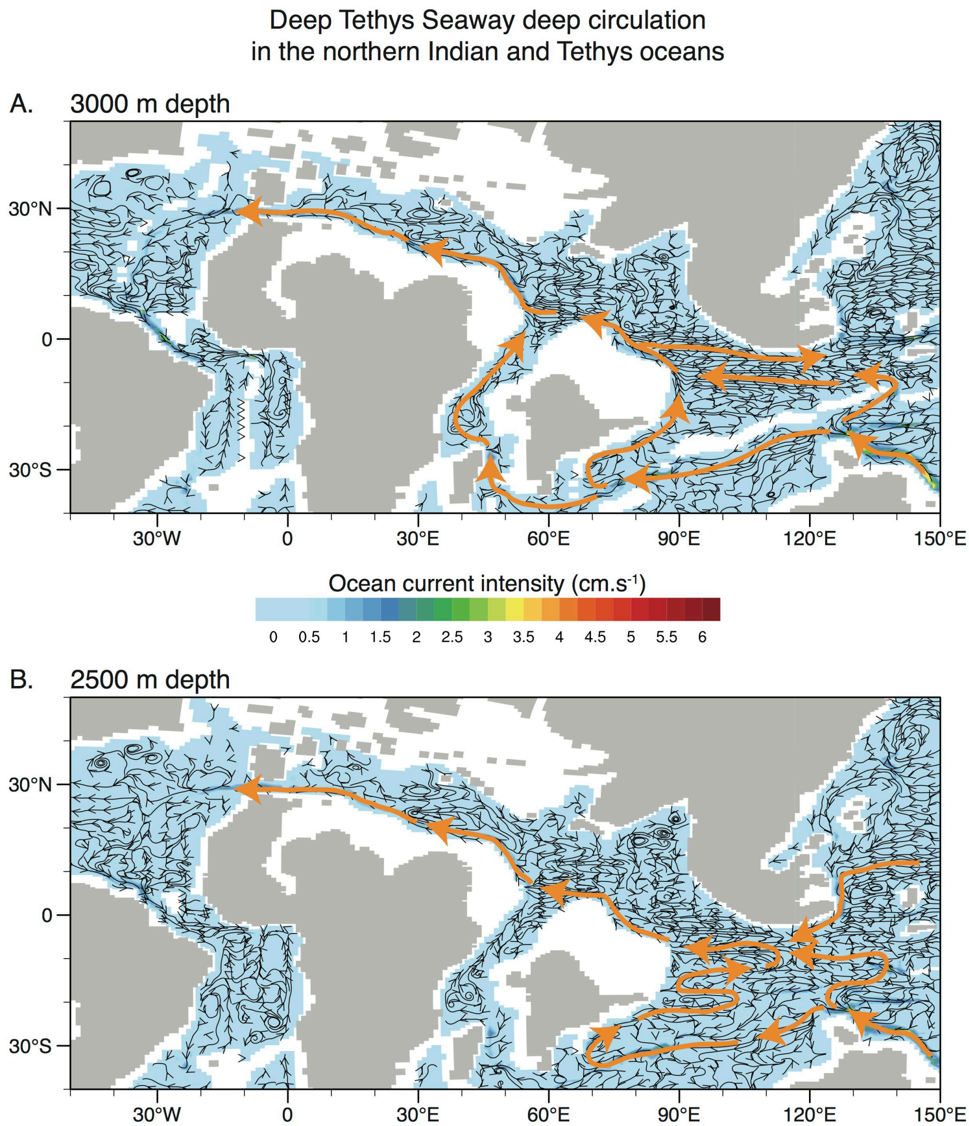

Figure 15. Deep Tethys Seaway deep ocean circulation in the northern Indian and Tethys oceans at (A) 3000 m depth and (B) 2500 m depth. Orange contours represent major pathways of water masses.

1467